A PRECISION MEASUREMENT OF FRESNEL DRAG IN A RING LASER

By

WALTER KENT STOWELL

Bachelor of Science
Oklahoma State University
Stillwater, Oklahoma
1970

Master of Science
Oklahoma State University
Stillwater, Oklahoma
1972

Submitted to the Faculty of the Graduate College
of the Oklahoma State University
in partial fulfillment of the requirements
for the Degree of
DOCTOR OF PHILOSOPHY
July, 1974

PREFACE

A precision measurement of the drag coefficient of light in a moving medium in a ring laser has been attempted and accomplished with unexpected results. One would expect the drag effect to follow one of the long standing theoretical models even in the ring laser, but the results of this work seem to indicate that all is not understood concerning this effect. In fact, none of the previously viable theoretical models explain completely the herein reported experimental results.

The experimental techniques used were basically those developed by Bilger and Zavodny (1972). Improvements were made in the experimental equipment and techniques that resulted in a substantial reduction in certain of the errors that existed in previous attempts at these measurements. Error reduction was approached mainly in the determination of the Brewster angle and the off-axis distance in the fused silica disk. Other errors were kept at a level set by Zavodny's experiments.

Only the experimental methods, techniques and equipment are discussed where they differ from the work reported by Zavodny (1970) in his Ph.D. dissertation, except where completeness requires otherwise. Suggestions for decreasing some of the uncertainty in the measurements are given. However, more importantly, suggestions are presented for the reduction of data scattering and possible errors due to signal processing.

In an endeavor of this nature there are many individuals who make contributions. In the light of this I would like to take this

opportunity to express my appreciation to the members of my committee: Dr. Hans R. Bilger, adviser and chairman, who suggested the problem and was always at hand when he was needed and seemed to have a mysterious catalog of solutions to offset my not so mysterious compliment of problems; Dr. Harold Fristoe, Dr. H. Jack Allison, and Dr. N. V. V. J. Swamy for their interest and assistance. I wish to acknowledge the advice and excellent craftsmanship of Mr. Heinz Hall, O.S.U. Physics Department machine shop, for his contributions to solving many mechanical problems encountered. I would like to express special appreciation to Mr. T. Joe Boehm for his many helpful suggestions regarding electronics problems encountered and for his continued encouragement, and Mr. Jawahar L. Tandon for his continued encouragement.

It is with great humility that I wish to express special appreciation to my wife, Beverly, for her understanding, encouragement and great personal sacrifices without which this dissertation would not have been possible.

Without regard to precedent I wish to dedicate my efforts in this endeavor to the incomparable Comte de Saint-Germain, my patron and of whom Voltaire, in a letter to Frederick II of Prussia, said ". . . he is a man who never dies, and who knows everything."

TABLE OF CONTENTS

LIST OF TABLES

LIST OF FIGURES

LIST OF SYMBOLS*

A	Area enclosed by the ring laser. (m^2)
$\mathring{A}$	Angstrom = 10^{-10} meter. (m)
b	General bias frequency due to the earth's rotation; hence, ordinate intercept for the plot of the equation $y = m_i x + b$. (Hz)
b_{exp}	Experimentally obtained value of b. (Hz)
Δb	General deviation of b from the best fitted curve $y = m_i x + b$.
Δb_{exp}	Deviation of b_{exp} from the best fitted curve $\Delta f_B = m_i f_m + b_{exp}$ or $\Delta f_B = m_i x_o + b_{exp}$. (Hz)
BZ	Published paper by Bilger and Zavodny (1972).
^oC	Celcius temperature. (degree Celcius)
C_i	Capacitance of quantity i. (Farad)
c	Velocity of light in vacuum. ($m\ sec^{-1}$)
d	Thickness of fused silica disk. (m)
dr	Line element along the beam path. (m)
f	Frequency of laser light. (Hz)
FET	Field effect transistor.
f_m	Rotation rate of fused silica disk. (RPM)
$\overline{f_m}$	The mean value of several values of f_m. (RPM)
$\overline{\overline{f_m}}$	The mean of several values of $\overline{f_m}$. (RPM)
Δf_B	Frequency separation of the contracirculating oscillators in a ring laser, i.e., beat frequency. (Hz)
$\overline{\Delta f_B}$	The mean value of Δf_B for the data considered. (Hz)
$\overline{\overline{\Delta f_B}}$	The mean of several values of $\overline{\Delta f_B}$. (Hz)

Δf_L	General frequency separation of axial modes in a ring laser. (Hz)
Δf_{Li}	Frequency separation of the axial modes in a ring laser, i = 1, 2, 3. (Hz)
K	Constant used in the text. (Units are defined in context used)
L	Optical path length of the ring laser oscillator cavity, ($\oint n\, dr = L$). (m)
LED	Light emitting diode.
L_i	Inductance of quantity i. (henry)
l	Optical path length through the fused silica disk. (m)
m_i	Slope of plotted curves of Δf_B vs. f_m or Δf_B vs. x_o where i = 0, 1, respectively. (Hz $(RPM)^{-1}$ or Hz $inch^{-1}$)
Δm_i	Deviation of data points from the slope m_i of the best fitted curve $y = m_i x + b$. (Hz $(RPM)^{-1}$ or Hz $inch^{-1}$)
M_i	Derived term proportional to m_i. (Hz $(RPM)^{-1} inch^{-1}$)
ΔM_i	Deviation of data points from M_i from the slope of the best fitted durve $y = m_i x + b$. (Hz $(RPM)^{-1} inch^{-1}$)
N	Integer value.
n	Index of refraction.
PD	Published paper by Parks and Dowell (1974).
q	Number of wavelengths around the complete ring laser optical path. (m)
r	Simple correlation coefficient.
RF	Radio frequency.
TEM_{mnq}	Mode designation in ring laser (modes with m = n = 0 are called axial modes).
u	Velocity of light in a moving medium as seen from an inertial (laboratory) reference frame. (m sec^{-1})
v	Velocity of the moving medium with respect to the inertial reference frame. (m sec^{-1})
v_I	Velocity component of the medium parallel to incident light. (m sec^{-1})

v_R	Velocity component of the medium parallel to the refracted light. (m sec^{-1})
T	Temperature. (^oC, degrees Celcius)
x	General horizontal position of the disk. (inch)
x_c	Center of rotation of the disk ($y_o = 0$). (inch)
x_o	Off-axial displacement of the laser beam relative to the axis of rotation. (inch)
y	General vertical position of the disk. (inch)
y_c	Center of rotation of the disk ($x_o = 0$). (inch)
y_o	Off-axial displacement in y-direction (see x_o). (inch)
Z_i	The impedance of a quantity i. (ohms)
α	General drag coefficient.
α_{exp}	Experimentally determined drag coefficient.
α_F	Fresnel drag coefficient.
α_{La}	Laub drag coefficient.
α_{Lo}	Lorentz modified drag coefficient (Fresnel drag coefficient modified by Lorentz to include dispersion).
θ	Latitude of the location of the experimental setup. (degrees)
θ_B	Brewster angle. (degrees)
θ'_B	Refracted angle of the incident light beam when the disk is at the Brewster angle. (degrees)
θ_i	Angle of incidence. (degrees)
θ_n	"Normal angle": angle between a normal to the surface of the optical flat and the plane which is both perpendicular to the plane of the ring and perpendicular to a line which is co-linear with the light beam. (degrees)
λ	Wavelength in vacuum. (m)
σ	Standard deviation of a quantity defined in context.
σ_a	Standard deviation of quantity a.
ω	Angular velocity. (rad sec^{-1})

Ω Angular velocity of the ring laser with respect to inertial space. (rad sec^{-1})

DELTA Δf_B Frequency difference between the observed value of Δf_B and the data fitted value of Δf_B. (Hz)

$dn/d\lambda$ Dispersion, i.e., rate of change of the index of refraction with wavelength. (m^{-1})

---

*Note that quantities that have an arrow ($\rightarrow$) over them are vector quantities and quantities having a bar ($-$) over them are average values.

CHAPTER I

INTRODUCTION

The intention of this study and the central aspect of this dissertation was to experimentally produce a precision determination of the Fresnel coefficient of drag of light which was first derived by Fresnel (1818), and compare the experimental results with the various existing theoretical models.

A more precise measurement of the light dragging effect is of interest because no one has proved conclusively which theory of the dispersion term should apply for the ring laser (closed light path and self-oscillating). Recently questions have surfaced as to whether the theoretical model used by Bilger and Zavodny (1972) was correct (Parks and Dowell, 1974, hereafter referred to as PD). PD's calculations give two possible results for the drag coefficient α both of which are within the experimental errors of Bilger and Zavodny. "The BZ [Bilger and Zavodny] experiment thus did not distinguish between the two dispersion terms to within experimental error" (PD, 1974, p. 566). There is an increase in interest in Fresnel drag measurement as a method of determining angular orientation in gyro-compass applications (Massey and Siegman, 1970). Any one of the above reasons renders further measurements of the Fresnel drag coefficient with increased precision desirable.

Significant History of the Drag Coefficient

The history of the investigation into the light dragging phenomenon is discussed in Zavodny's dissertation (Zavodny, 1970) and concisely summarized in a paper by Bilger and Zavodny (1972); therefore, it will be dealt with only briefly here. The history of the drag coefficient which appeared in the BZ paper is reproduced (with permission of the author) here as Table I with the addition of the results of Zavodny's work.

Zavodny (1970), using a ring laser at a wavelength of 0.633 μm (Comité International des Poids et Mesures (1973)) was able to measure the drag coefficient with a "total error due to random input data and known systematic error sources kept below 0.6%" (Zavodny, 1970).

Experimental Method

Basically the experimental techniques that were devised by BZ were used in the determination of the drag coefficient. An improvement in the precision of the drag measurements required that certain of the equipment and techniques be changed. The drag site (platform for holding the rotating fused silica disk) was completely redesigned with more massive construction. Also an extremely accurate x-y translator was added for changing the position of the rotating fused silica disk in the ring laser cavity. A new technique for setting the disk at its Brewster angle was developed. A factor of 10 or better improvement was made both in setting the Brewster angle and in adjusting and reading the off-axis distance of the fused silica disk. The other known error sources were kept at a level equal to or below those of Zavodny. All

TABLE I*

HISTORY OF THE DRAG COEFFICIENT

Year	Investigator	Contribution		Comment
1818	Fresnel	$\alpha_F = 1 - (1/n^2)$	Theor.	Correct result (without dispersion term), but wrong theory
1851	Fizeau	$\alpha/\alpha_F = 1.14 \pm ?$	Expt.	In water; error probably larger than ±0.14
1886	Michelson Morley	$\alpha/\alpha_F = 0.993 \pm 0.05$ ($\alpha/\alpha_F = 0.964 \pm 0.05$)	Expt.	In water
1895	Lorentz	$\alpha_{Lo} = 1 - (1/n^2) - (\lambda/n)(dn/d\lambda)$	Theor.	Inclusion of dispersion term
1907	Laue	Derivation of α_F by relativistic addition theorem	Theor.	
1914	Einstein	Explanation of dispersion term by Doppler effect	Theor.	
1914-1925	Zeeman	$\alpha/\alpha_{Lo} = 0.998 \pm 0.006$	Expt.	In water and fused silica at different wavelengths; confirms dispersion term
1970	Zavodny	$\alpha = 0.541 \pm 0.003$ $\alpha/\alpha_{Lo} = 0.998 \pm 0.006$ $\alpha/\alpha_{La} = 1.005 \pm 0.006$	Expt.	Fused silica in ring laser

*Bilger and Zavodny, 1972, p. 593.

data were taken using the same fused silica disk that Zavodny used for direct comparison purposes.

Results Obtained

The average of seventeen determinations of the drag coefficient was $\bar{\alpha}_{exp} = 0.5425$. The total error in $\bar{\alpha}_{exp}$, due to statistics and estimates of systematic errors, is set to $\sigma_{\bar{\alpha}_{exp}} = 0.0004$.

The earth's rotation produces a bias (due to the Sagnac effect) in the ring laser which was accounted for in the experimental results. This bias shows up in the data as a shift in the beat frequency. The experimental value of this bias was $b_{exp} = 48$ Hz ±2 Hz, which is within 4 Hz of the theoretical value of $b = 44$ Hz as computed for the particular location of the experiment. A detailed discussion of the existing theoretical models for the drag coefficient will be covered in Chapter II, but as a point of information we note here that only the Lorentz-type drag equation produces a result which is numerically close to the observed $\bar{\alpha}_{exp}$. In fact the Lorentz modified drag coefficient (referred to hereafter as α_{Lo}) compares with α_{exp} as follows:

$$1.0004 \leq \frac{\alpha_{exp,\,i}}{\alpha_{Lo}} \leq 1.0039; \quad i = 1,2,\ldots,17 \qquad (1\text{-}1)$$

and for the average $\bar{\alpha}_{exp}$ and its estimated uncertainty we have

$$\frac{\bar{\alpha}_{exp}}{\alpha_{Lo}} = 1.0018 \pm 0.0007 \; . \qquad (1\text{-}2)$$

CHAPTER II

THEORETICAL TREATMENT

Introduction

The theory of the ring laser and Fresnel drag as well as a complete derivation of equations describing these phenomena has been thoroughly treated in Zavodny's thesis (1970) and the BZ paper. It has been satisfactorily established, by Zavodny's results, that the Fresnel model of the drag coefficient does not describe completely the dragging effect in a ring laser. Therefore, we shall confine the theoretical discussion to the question set down by the PD paper, namely that the results of Zavodny's experiments "did not distinguish between the two dispersion terms to within experimental error" (PD, 1974, p. 566). Note that the two dispersion terms mentioned refer to the Lorentz dispersion term and that of Laub (1908).

Existing Viable Theoretical Models

The PD paper lucidly discusses the conditions of the experimental arrangement that existed in the BZ experiment which are identical to those in this present study, namely; (a) the laser light beam was incident at the Brewster angle of a fused silica disk, and (b) the velocity vector $\vec{v}$ is perpendicular to the surface normal (see Figure 1).

Through use of the Doppler effect and relativistic velocity addition concepts PD arrive at a generalized expression for the velocity of

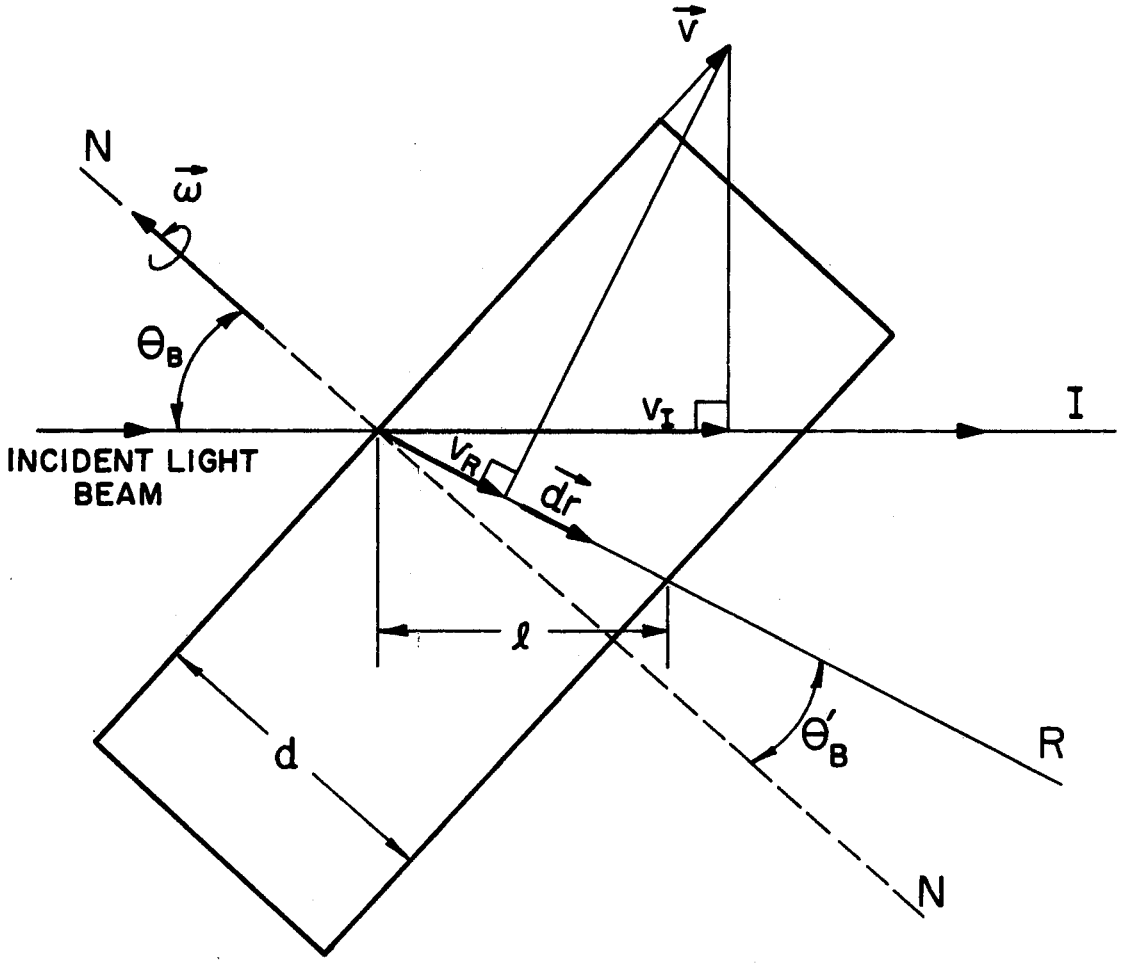

Figure 1. Diagram of Drag Disk Depicting the Direction of the Incident Beam I and Refracted Beam R

light in the moving medium u as seen from the inertial reference frame.

$$u = \frac{c}{n(\lambda)} - v_I \frac{\lambda}{n^2(\lambda)} \frac{dn(\lambda)}{d\lambda} + v_R \left(1 - \frac{1}{n^2(\lambda)}\right) \tag{2-1}$$

where c = vacuum velocity of light

$n(\lambda)$ = index of refraction of the moving medium as a function of wavelength

v_I = velocity component of the moving medium parallel to direction of incident light

v_R = velocity component of the moving medium parallel to direction of refracted light

λ = vacuum wavelength of light beam

By resolution of the velocity vector $\vec{v}$ (see Figure 1) in the direction of both the incident light v_I and refracted light v_R and through use of Snell's law one can show that

$$v_I = n(\lambda)\, v_R \tag{2-2}$$

Equation (2-1) reduces rapidly to

$$u = \frac{c}{n(\lambda)} + \left(1 - \frac{1}{n^2(\lambda)} - \frac{\lambda}{n(\lambda)} \frac{dn(\lambda)}{d\lambda}\right) v_R \tag{2-3}$$

which can be written as

$$u = \frac{c}{n(\lambda)} \pm \alpha v_R \,. \tag{2-4}$$

Equation (2-3) is the Lorentz formula and Equation (2-4) then defines the Lorentz drag coefficient

$$\alpha_{Lo} = 1 - \frac{1}{n^2(\lambda)} - \frac{\lambda}{n(\lambda)} \frac{dn(\lambda)}{d\lambda} \,. \tag{2-5}$$

PD also considered another case where $v_I = v_R = v$ (v is the magnitude of the velocity of the moving medium) and Equation (2-1) reduces to the Laub formula

$$u = \frac{c}{n(\lambda)} + \left(1 - \frac{1}{n^2(\lambda)} - \frac{\lambda}{n^2(\lambda)} \frac{dn(\lambda)}{d\lambda}\right) v \,. \tag{2-6}$$

We see then that the Laub drag coefficient α_{La} is

$$\alpha_{La} = 1 - \frac{1}{n^2(\lambda)} - \frac{\lambda}{n^2(\lambda)} \frac{dn(\lambda)}{d\lambda} \tag{2-7}$$

It must be kept in mind that the above formulation does not take into account the specifics of the ring laser. These relationships are based on a passive light beam incident upon a moving medium, whereas, with the ring laser the moving medium is placed inside the active cavity of the light source.

Drag in a Ring Laser

Post (1967) gives an equation for the beat frequency (which is also mentioned in BZ) for a stationary ring laser and moving medium in the beam path as

$$\Delta f_B = \left(\frac{2f}{c}\right) \frac{\oint n^2 \alpha \vec{v} \cdot d\vec{r}}{\oint n \, dr} \tag{2-8}$$

where $\oint n \, dr = L$ = optical path length of the ring cavity

dr = line element along the beam path

$f = c/\lambda$ = frequency of light beam

α = coefficient of drag

c = vacuum velocity of light

$\oint \vec{v} \cdot d\vec{r} = v_R l$ for our case, see Figure 1. The fused silica disk is the only moving medium in the beam path with the inside path length l.

Note that the optical length of the ring laser is evaluated (see Chapter IV) through a measurement of the axial mode separation Δf_L where $\Delta f_L = c/L$. For the special case of our experiment (as stated by BZ) Equation 2-8 is

$$\Delta f_B = \frac{2 n^2 \alpha f v_R l}{L c} = \frac{2 n^2 \alpha v_R l}{\lambda L} \, , \tag{2-9}$$

Through use of Brewster's law we get (assuming the disk is tilted at the Brewster angle θ_B and the normal angle of the tilt (see Chapter III) is 90°)

$$v_R 1 = \frac{\omega d x_o}{n} \tag{2-10}$$

where $\omega = 2\pi f_m$, where f_m is the rotation rate of the disk

x_o = off-axial displacement of the laser beam relative to the axis of rotation.

With Equation (2-10), Equation (2-9) gives the beat frequency due to drag in a rotating disk as

$$\Delta f_B = \frac{4\pi d n \alpha x_o f_m}{\lambda L} . \tag{2-11}$$

Evaluation of the Drag Coefficient

The beat frequency due to both the drag and Sagnac effect can be written as

$$\Delta f_B = \frac{4\pi d n \alpha x_o f_m}{\lambda L} \pm \frac{4 \vec{A} \cdot \vec{\Omega}}{\lambda L} \tag{2-12}$$

where A = enclosed area of the ring laser

Ω = angular velocity of the ring laser with respect to inertial space

and the other symbols are defined above. The Sagnac effect should be included since the ring laser rotates with the rotating earth.

In actual practice the beat frequency Δf_B was measured as a function of rotation rate of the disk f_m and displacement of the beam from the center of rotation of the disk x_o, (details given in Chapter V). Differentiating Equation (2-12) with respect to f_m yields

$$\frac{d(\Delta f_B)}{d f_m} = m_o = \left(\frac{4\pi d n x_o}{\lambda L}\right) \alpha \qquad (2\text{-}13)$$

and differentiation of Equation (2-12) with respect to x_o yields

$$\frac{d(\Delta f_B)}{d x_o} = m_1 = \left(\frac{4\pi d n f_m}{\lambda L}\right) \alpha , \qquad (2\text{-}14)$$

which allows us to use the numerical values of the slopes m_o and m_1 of the plotted curves to obtain α as follows:

From Equation (2-13) we write

$$\alpha = \left(\frac{\lambda L}{4\pi d n x_o}\right) m_o \qquad (2\text{-}13a)$$

or, in the units used in the experiments

$$\alpha = 1.87978 \times 10^2 \left(\frac{\lambda(m)\, L(m)}{d(m)\, n\, x_o(in)}\right) m_o \left(\frac{Hz}{RPM}\right) \qquad (2\text{-}13b)$$

and Equation (2-14) is rearranged as

$$\alpha = \left(\frac{L}{4\pi d n f_m}\right) m_1 \qquad (2\text{-}14a)$$

or, in the units used in the experiment

$$\alpha = 1.87978 \times 10^2 \left(\frac{\lambda(m)\, L(m)}{d(m)\, n\, f_m(RPM)}\right) m_1 \left(\frac{Hz}{in}\right) . \qquad (2\text{-}14b)$$

The drag coefficient α may be evaluated through either Equation (2-13b) or Equation (2-14b). In general, Equation (2-12) is now written as

$$\Delta f_B = m_o f_m + b, \qquad (x_o = \text{constant}) \qquad (2\text{-}15)$$

or

$$\Delta f_B = m_1 x_o + b, \qquad (f_m = \text{constant}) \qquad (2\text{-}16)$$

with $b = \frac{4\vec{A}\cdot\vec{\Omega}}{\lambda L} = \frac{4 A \Omega}{\lambda L} \sin\theta$, (see Equation (2-12), θ = latitude of the location of the experimental setup = $37^{o}7'$).

CHAPTER III

EXPERIMENTAL APPARATUS

Introduction

The particular configuration of the ring laser used in these experiments was designed and constructed by Zavodny (1970). Only the changes to the existing system or techniques will be reported here except where completeness requires otherwise. A block diagram of the ring laser and support equipment is shown in Figure 2. Discussed in this chapter are: the ring laser and beam combiner, the beat frequency detection system, the signal processing and data accumulation, the drag site which includes the rotator assembly, the rotation rate measuring system and equipment used for measuring the optical length of the ring.

Ring Laser Equipment and Beam Combiner

New mirror reflectors were purchased with reflectances of 99.9+% as specified by the manufacturer. Mirrors with a 1 m radius of curvature were used at the corners near either end of the plasma tube and a mirror with a 2 m radius of curvature was used at the output corner. The output mirror had a transmittance of approximately 0.1%. Several new plasma tubes were purchased but it was found that the same PEK Labs tube used by Zavodny (1970) worked best for the visible 0.633 μm transition line of the He-Ne laser. The plasma tube had to be "rejuvenated" several times, over a period of two years, by placing it in a

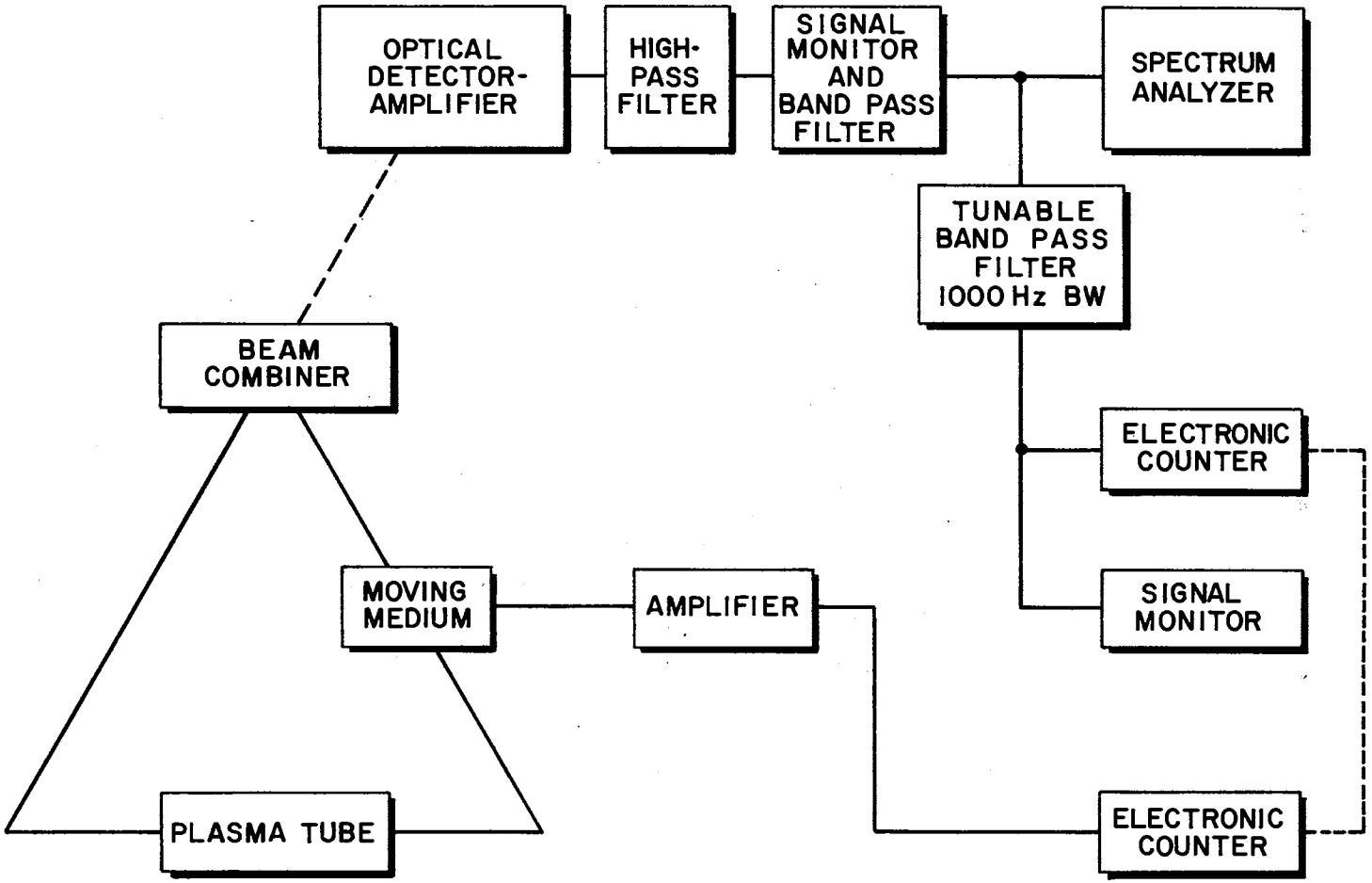

Figure 2. Block Diagram of the Equipment Configuration for Measuring Beat Frequency vs. Rotation Rate or Off-Axis Distance

helium bath at atmospheric pressure for up to 24 hours at a time. This procedure increased the He-pressure in the tube through backdiffusion.

The plasma tube had no internal electrodes and required RF excitation which was accomplished by placing narrow copper strips around the tube. They were alternately connected to two long 10 gauge (AWG) copper wires (see Figure 4). One of the wires was grounded and the other connected to a matching network (see Figure 3). The strips were evenly spaced to provide even excitation and reduce thermal gradients in the tube. RF power of approximately 30 W was supplied by a Viking Challenger amateur radio transmitter with less than 1 W reflected power. Considerable time was spent in reducing the reflected power by improving the matching network between the transmitter and plasma tube. The impedance, Z_{tube}, of the plasma tube was found to be on the order of 10 kΩ. The inductor, L_1, (see Figure 3) was set 4 μh and the capacitors were adjusted for minimum power reflected back to the transmitter.

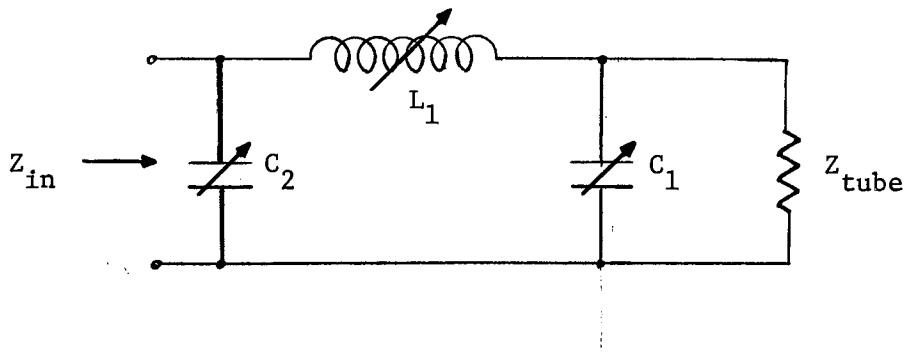

Figure 3. Impedance Matching Network Between Transmitter and Plasma Tube

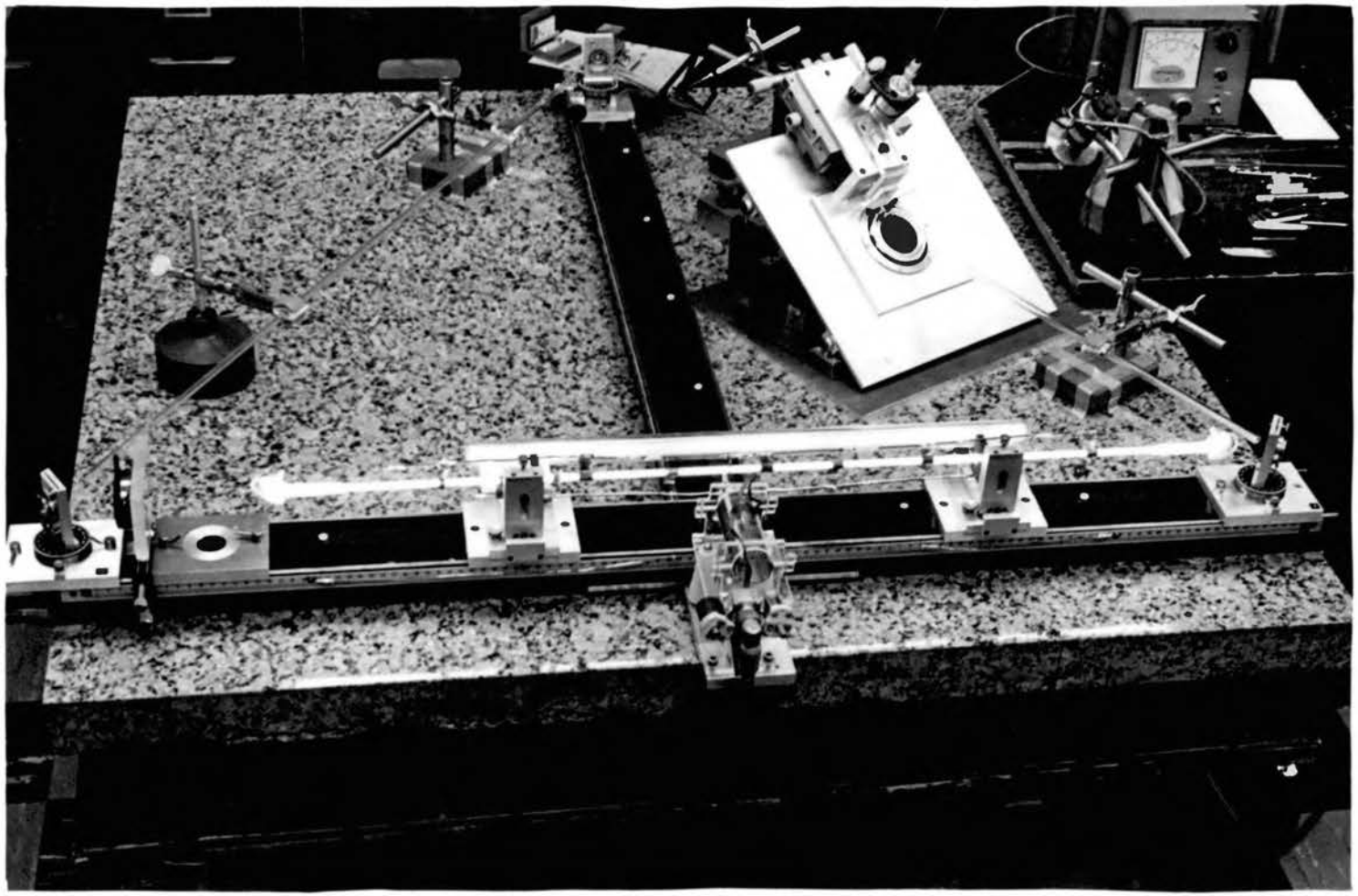

Figure 4. Ring Laser and Granite Table Top

Alignment of the ring laser was achieved with an auxiliary system using a 1 mW laser by reflecting the beam into the ring cavity and aligning the mirrors. A discussion of the laser mirrors and their holders is ably done in Zavodny's thesis (1970).

An iris located between one end of the plasma tube and the nearest mirror (see Figure 4) was used to introduce sufficient losses in the ring to insure pure axial mode (TEM_{ooq}) operation. Further reduction of the iris opening and also of the output power of the transmitter allows one to reduce the gain such that one oscillating axial mode persists.

To insure that indeed only one axial mode was oscillating, the frequency range where the lowest mode beat frequency would appear was monitored periodically on a spectrum analyzer in the same setup that was used in the ring optical length measurements (see end of this chapter). While monitoring, one simply had to look for the absence of a pip on the spectrum analyzer in the frequency range mentioned.

The granite table on which the laser was located along with the supporting table are adequately discussed in Zavodny's thesis. Also for a description of the beam combiner one is referred to Zavodny's thesis except for one improvement. The mass of the front surface mirror mount (see Figure 5) had to be increased in an effort to decrease the vibration in the beam combiner. It would be a serious source of instability if only one of the beams was subjected to a vibrating surface. To check for any vibration, a small Michelson interferometer was set up in which the front surface mirror in the beam combiner served as one of the mirrors in the interferometer. The quartz disk rotator and drive system was then operated to see if this caused a shifting of the fringes of the

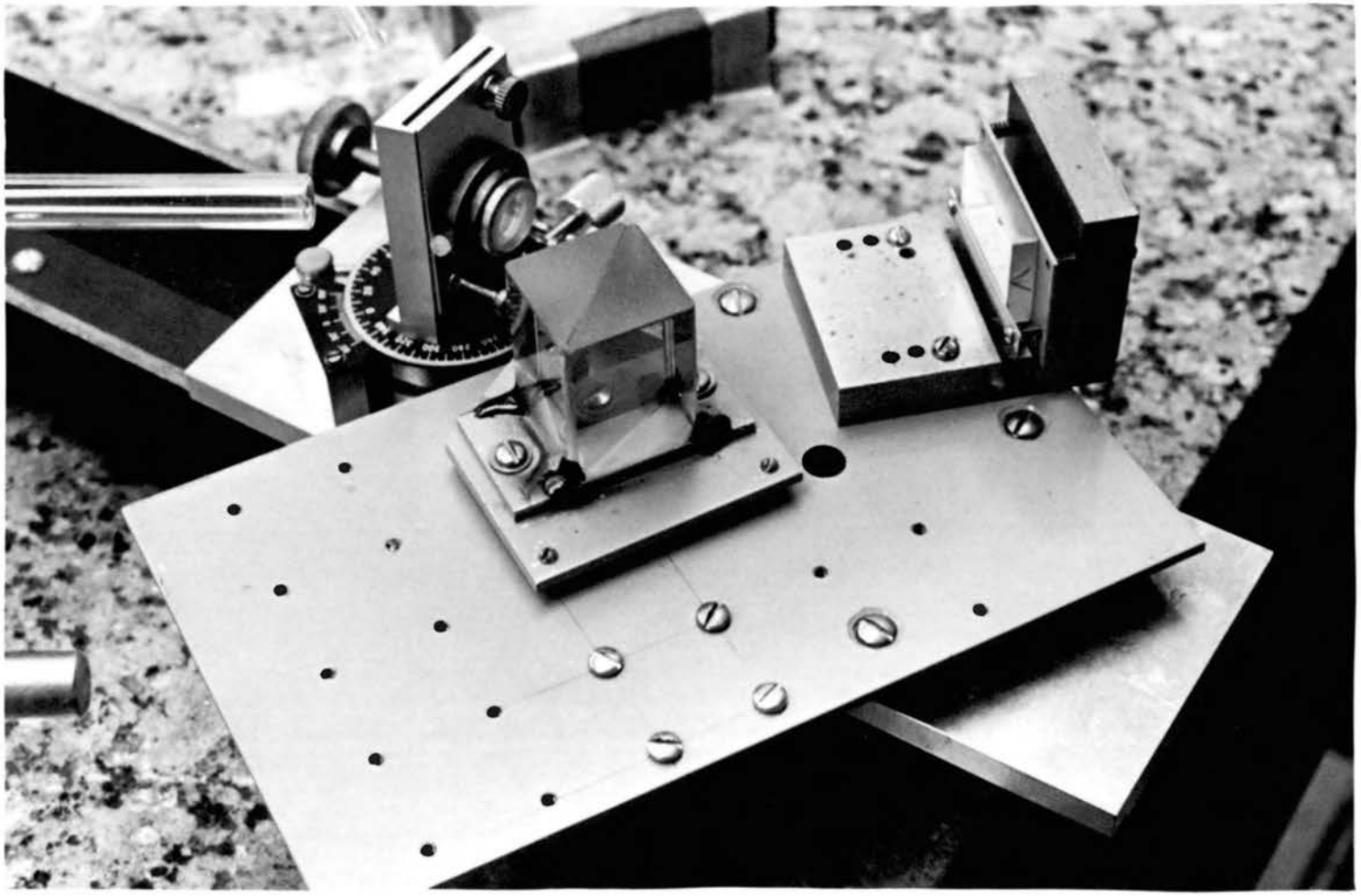

Figure 5. Beam Combiner

interferometer. It was found that with the existing mirror mount there was considerable vibration being transmitted to the front surface mirror. The more massive mount decreased but did not eliminate the observable vibration. In addition to the front surface mirror being adjustable, the beam splitter was mounted so that it could be aligned to be perpendicular to the clockwise beam and could be tilted to allow the two beams to be exactly (to the extent it was observable) coincident and parallel. Alignment of the beam combiner was accomplished in a manner not different to that reported by Zavodny (1970).

Beat Frequency Detection System

A schematic diagram of the detector and preamplifier circuit that was used to drive a high-gain amplifier is shown in Figure 6. The high-gain amplifier was manufactured by Electro-Nuclear Laboratory Model 303. The detector used was a Fairchild FPM200 silicon planar passivated photodiode. The bandwidths of the preamplifier and the high-gain amplifier were 3.5 MHz and 1 MHz respectively. Ultra-low-noise E8000 FETS manufactured by Texas Instruments were used in the preamplifier. The detector, preamplifier, and high-gain amplifier were all mounted in a small aluminum box with a small hole drilled in one end for the detector. The signal to noise ratio of the detector system was measured by modulating a Fairchild FLD100 LED (emission peaks at $\lambda = 0.9$ μm) in an already existing system. The output power of the LED as measured with an Optics Technology Model 610 power meter, was of the order of 5 μW near the surface of the LED window. A double convex lens, 35 mm diameter and 70 mm focal length, was placed 8 cm from the LED and the detector box was rigidly clamped to an optical bench 2.5 meters from the

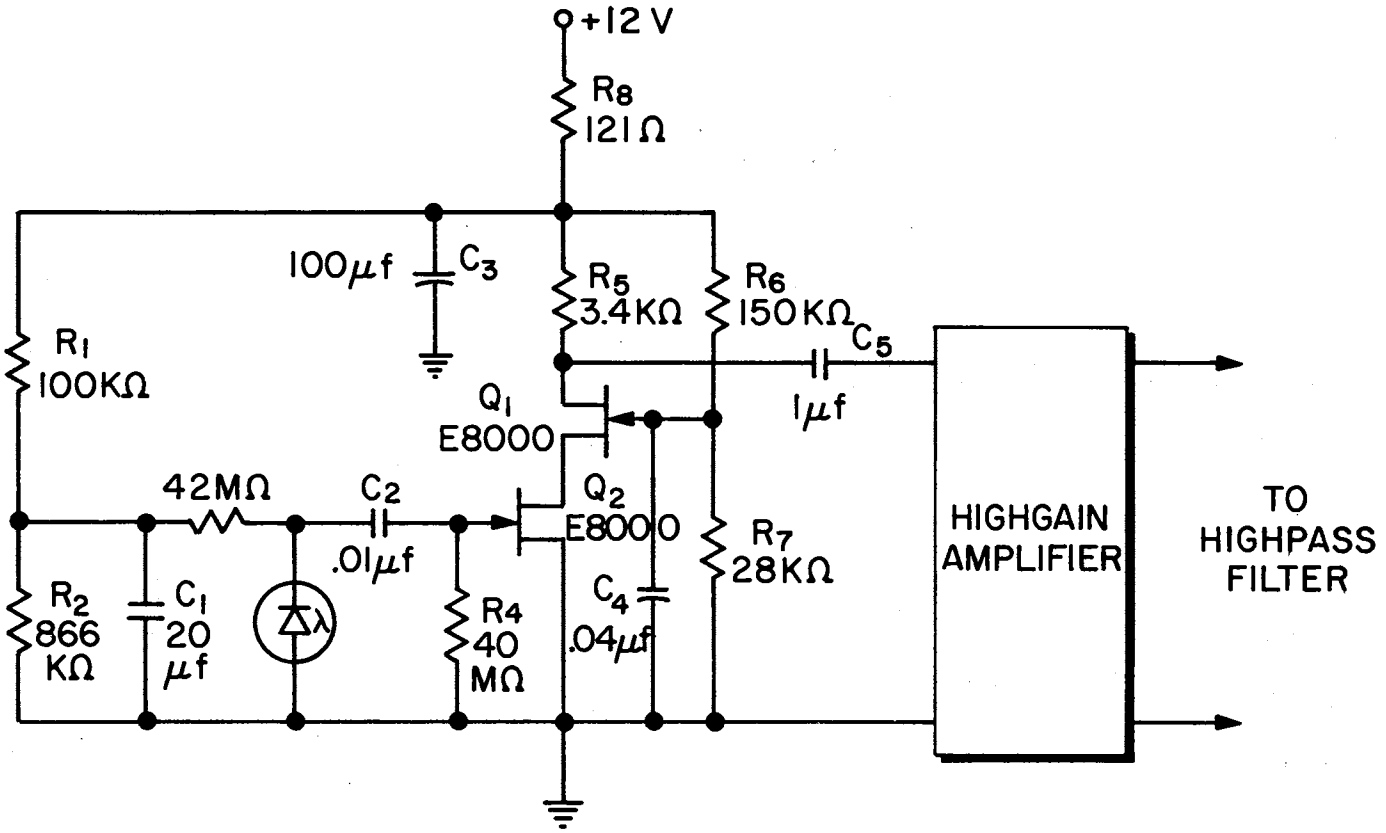

Figure 6. Schematic Diagram of Beat Frequency Detector and Preamplifier

lens. Measurements were taken at 100 Hz, 1 kHz and 10 kHz using a Tektronix 547 oscilloscope with a type 1A7A plug-in unit for bandwidth selection. The minimum signal to noise ratio was found to be 30 and the maximum 120. In the frequency range that the beat frequency occurred, it was possible to detect a signal as low as two nanowatts. This detector-amplifier system proved to be more than adequate to detect the drag signal.

In practice, the optical detector was located away from the laser platform at a distance of about 2 meter.

Beat Frequency Signal Processing Section

As was mentioned in the section on the optical detector, the light amplitude incident on the photodiode was converted into a voltage signal and amplified in the detector-amplifier. This signal was then fed into an active high-pass filter (see Figure 7) that had a 24 db per octave roll-off with a corner frequency of 500 Hz. There was no beat frequency information lost due to this filtering process because the lock-in frequency of this particular ring laser setup was approximately 500 Hz.

The output of the high-pass filter was observed on a Tektronix 547 oscilloscope with a Type 1A7A plug-in unit. The 1A7A plug-in unit has a bandpass filter incorporated in it that allows one to change the high and low cutoff frequencies which served quite well in reducing noise and eliminating spurious pickup. The band limit settings, on the 1A7A plug-in, actually set the 3 db down points for the high and low ends of the bandwidth and in practice were set at 300 kHz and 100 Hz, respectively. The low end overlapped with the high-pass filter providing an added measure of filtering for 60 Hz hum. The output of the 1A7A

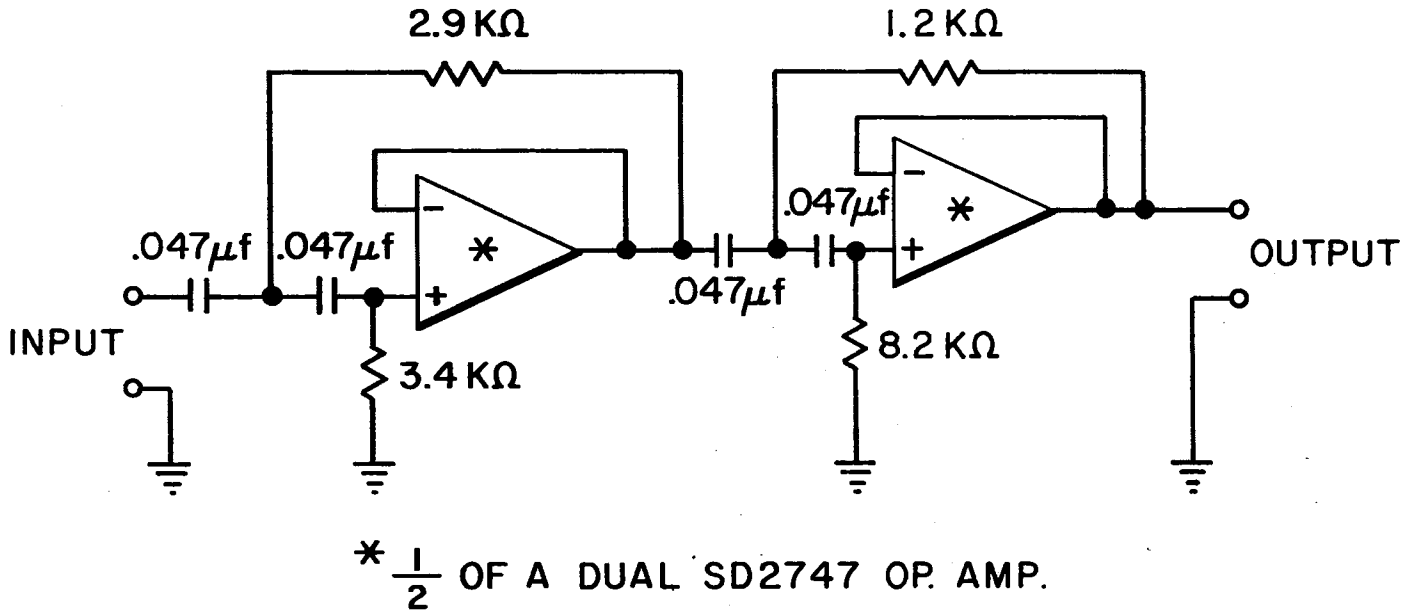

Figure 7. Schematic Diagram of the High-Pass Filter

plug-in, being a slightly filtered version of the input, was monitored on a Singer Panoramic Universal Spectrum analyzer Model MF-5 with a Module UR-3 plug-in unit and simultaneously fed to a Hewlett-Packard Model 310A wave analyzer. The analyzer was used as a tunable narrow band filter utilizing the 1 kHz bandpass setting. To insure that an adequate beat frequency signal was always present at the input to the electronic counter (see Figure 1), the signal level from the wave analyzer was monitored continuously on a Tektronix 585 oscilloscope. This signal monitor was maintained in addition to the spectrum analyzer.

Data Accumulation Equipment

The beat frequency Δf_B was counted by a General Radio Type 1151-A electronic counter and the rotation rate signal f_m was counted by a General Radio Type 1150-BP electronic counter. In order to have the two signals counted over identical time periods, the time base of the Type 1151-A counter was used for both counters. Provisions were provided for this connection between counters but because of a mismatch of impedance a slight modification was performed on the Type 1151-A (see Figure 8). This counter also supplied trigger and reset pulses for both GR counters. A comparison of the GR counters with a third counter (HP524D, see equipment list and ring optical length measurement) showed that at 50 kHz they were within $0.2 \times 10^{-4}\%$ of each other, and at 350 kHz they were within $0.8 \times 10^{-3}\%$ of each other. A Tektronix Type 190B constant amplitude signal generator was used to make this check. Note that it was necessary to stay within the bandwidth of the GR counters (400 kHz). The two GR counters always gave the same count ±1 count regardless of the frequency (within their bandwidth) being counted. To get an actual

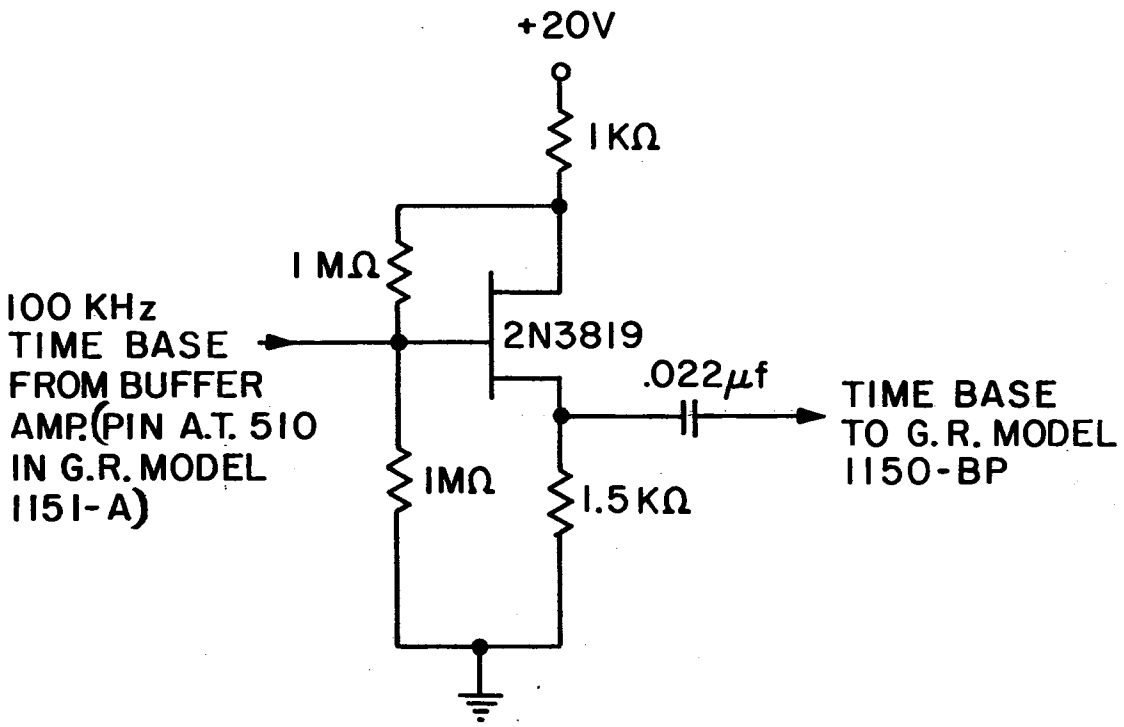

Figure 8. Schematic Diagram of the Time Base Impedance Matching Modification of the General Radio Model 1151-A Counter

check of the accuracy of these counters, one would have to count the frequency of a calibrated frequency standard. The minimum trigger level for the GR counters was 0.1 volts. The rotation rate signal was typically 6 volts peak to peak. The beat frequency Δf_B was continuously monitored for proper amplitude. This signal monitor allowed reliable adjustments to be made in the amplifier-filter system to insure that acceptable signal levels were always present at the counter input. It is interesting to note that since the counters used to count Δf_B and f_m are synchronized by the same time base, an error in the time base cancels out in the determination of the drag coefficient α (see Equation 2-13). Figure 9 shows the relative positions of the equipment; note that the two GR counters are located at the top of the vertical relay rack.

Drag Site Preparation

The method of obtaining the linear velocity component, of the fused silica disk, parallel to the laser beam was identical to that used by Zavodny which was originally used by Macek et al. (1964). This method will be described briefly here for completeness.

The fused silica optical flat was placed in a bearing mounted holder which was then mounted on an adjustable platform in such a manner that the flat could be rotated and translated horizontally and vertically. The inclination angle of the platform was adjusted with a micrometer that had an accuracy of 0.01 mm. The horizontal or vertical (x or y, respectively) position of the optical flat could be adjusted by micrometers with a resolution of 1×10^{-4} inch. The platform that held the rotator assembly is shown in Figure 10 and Figure 11.

Figure 9. Equipment in the Configuration Used While Taking Beat Frequency Measurements

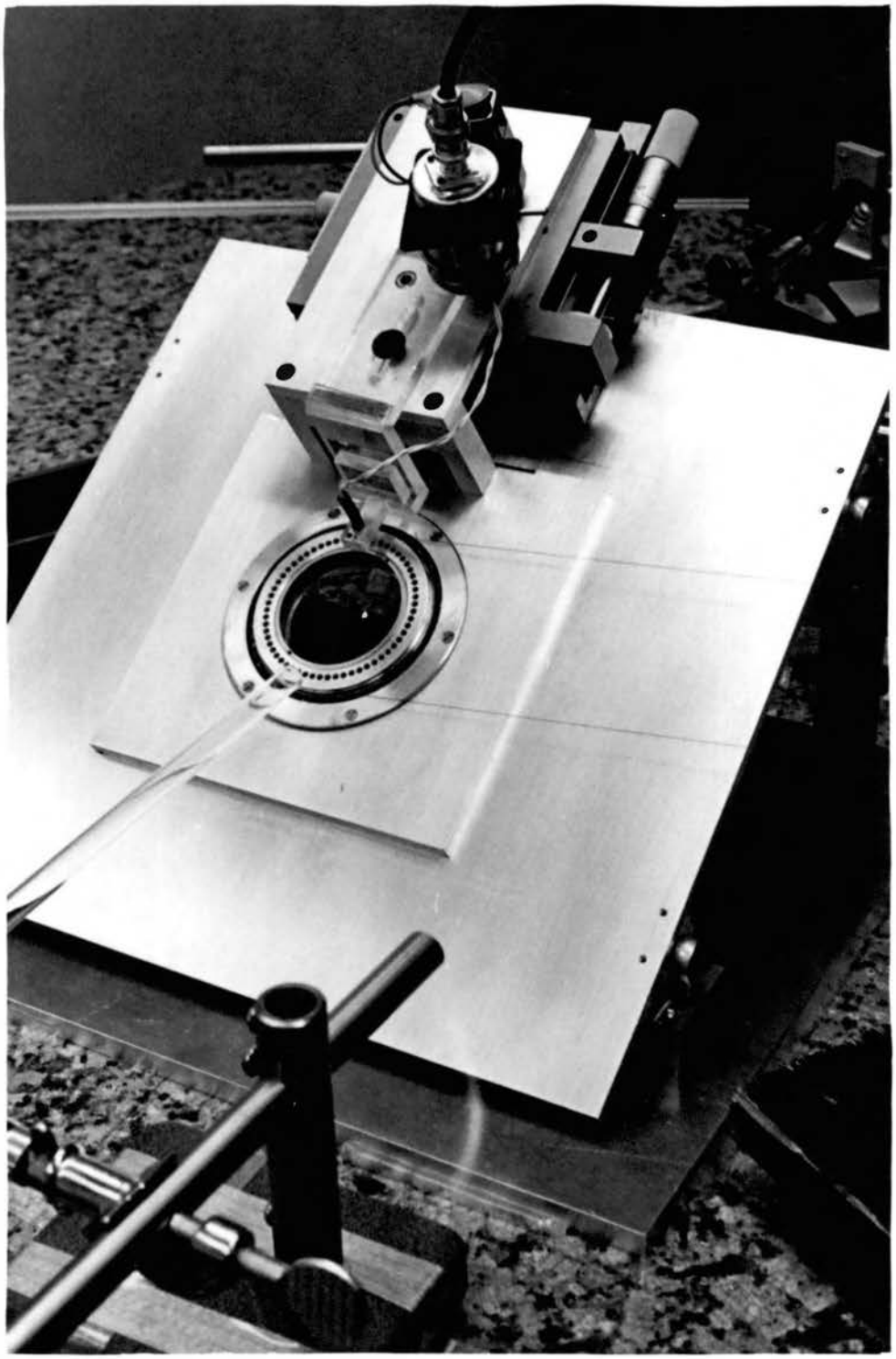

Figure 10. Front View of Drag Platform

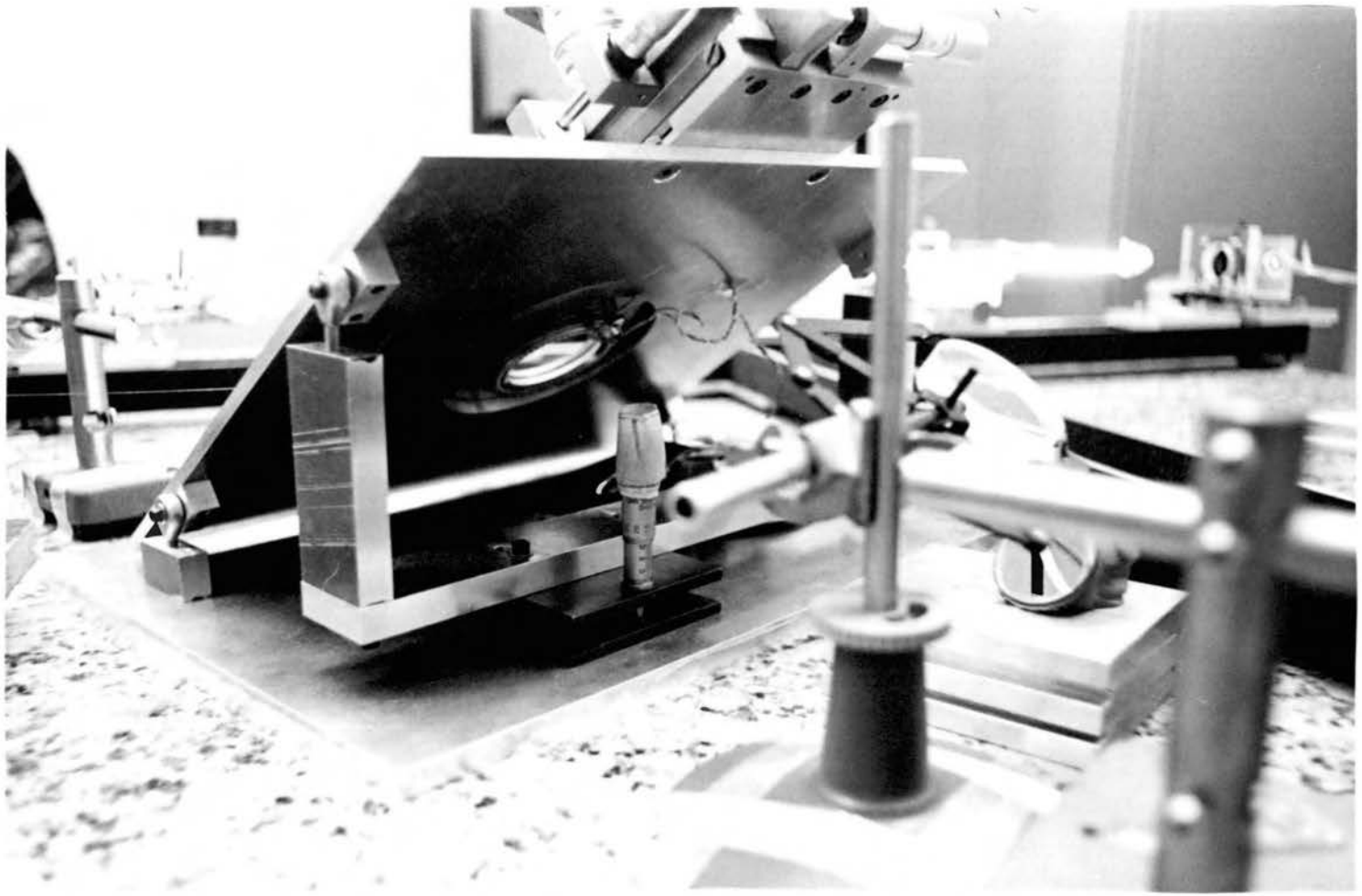

Figure 11. Rear View of Drag Platform Showing Sine Table Adjustment

The wooden table and granite slab were leveled by using a 1 m long machinist level as an indicator and adjusting the spring tension on the supporting feet. The normal angle θ_n adjustment was made prior to fixing the drag site to the granite slab. This angle, θ_n, is 90^o when the normal to the surface of the optical flat was set in a vertical plane defined by a line on the ceiling above the ring and the laser beam in the arm of the ring that contained the drag site. The line on the ceiling was drawn through several points obtained by plumbing the beam path from the ceiling (a distance of approximately 2.1 m) and drawing a straight line on the ceiling through the plumb points. The ring laser beam was then made to reflect to the ceiling off the face of the mounted optical flat. This reflected spot on the ceiling was made coincident with the line drawn on the ceiling by positioning the entire platform and base plate. When the spot and line were coincident, the platform base plate was fixed to the table top with a silicone sealing compound manufactured by General Electric. The distance from the reflection point on the fused silica disk to the spot on the ceiling was 2.3 m and the maximum possible deviation off the line (i.e., spot diameter) was ±1.5 mm; hence, the normal angle was adjusted to within 5 minutes of arc. The error introduced in α by an error in the normal angle is a second order error. It can be shown that an error of 5 minutes of arc introduces an error in α of less than 1.6×10^{-4}%, which is negligible compared to other errors. The beat frequency detector was located off and approximately 2 m away from the beam combiner. The diameter of the beam at the optical detector was approximately 1 mm (the intensity of the beam was at a minimum while taking beat frequency measurements, therefore, the spot diameter was also). The diameter of the sensitive area

of the photodiode was approximately 1 mm. This would mean that if the table tilted, while taking data, more than 3.5 minutes of arc it would show up in a loss of the beat frequency signal. Admittedly the axis of tilt that would cause a loss of signal is not the same axis as that which would cause a maladjustment in the normal angle but one would hardly expect the table to tilt about only one special axis. In the light of the above, it was assumed that the vertical plane defined by the line on the ceiling and the laser beam was normal to the plane of the ring.

A duplicate of the diagram of the rotator and optical flat that was presented by Zavodny is included here as Figure 12 for completeness. The front and rear views of the drag site are shown in Figure 10 and Figure 11. Note that in Figure 11 one can see the placement of the compensator flat, also the sine table and micrometer which was used to adjust the inclination angle of the platform. Figure 10 shows the front view of the drag site where one can see the x-y translator and the rotator with drag disk in place.

The same type of ball bearing was used but a new one was purchased from Split Ball Bearing Company as Model 3TKR41-52-U. The same type lubricant (tungsten diselenide as lubricant #1433 from Cerac, Inc.) was used, however, a somewhat different lubrication procedure was followed. The bearing was cleaned with naptha, then we lightly burnished all exposed ball surfaces. One method that worked quite well was to spread a few grams of the lubricant out on a card or piece of paper (an IBM card worked very well) using a small artist's paint brush, then pouring the lubricant back into the container just lightly tapping the edge of the card. The lubricant that remains on the card is then brushed up

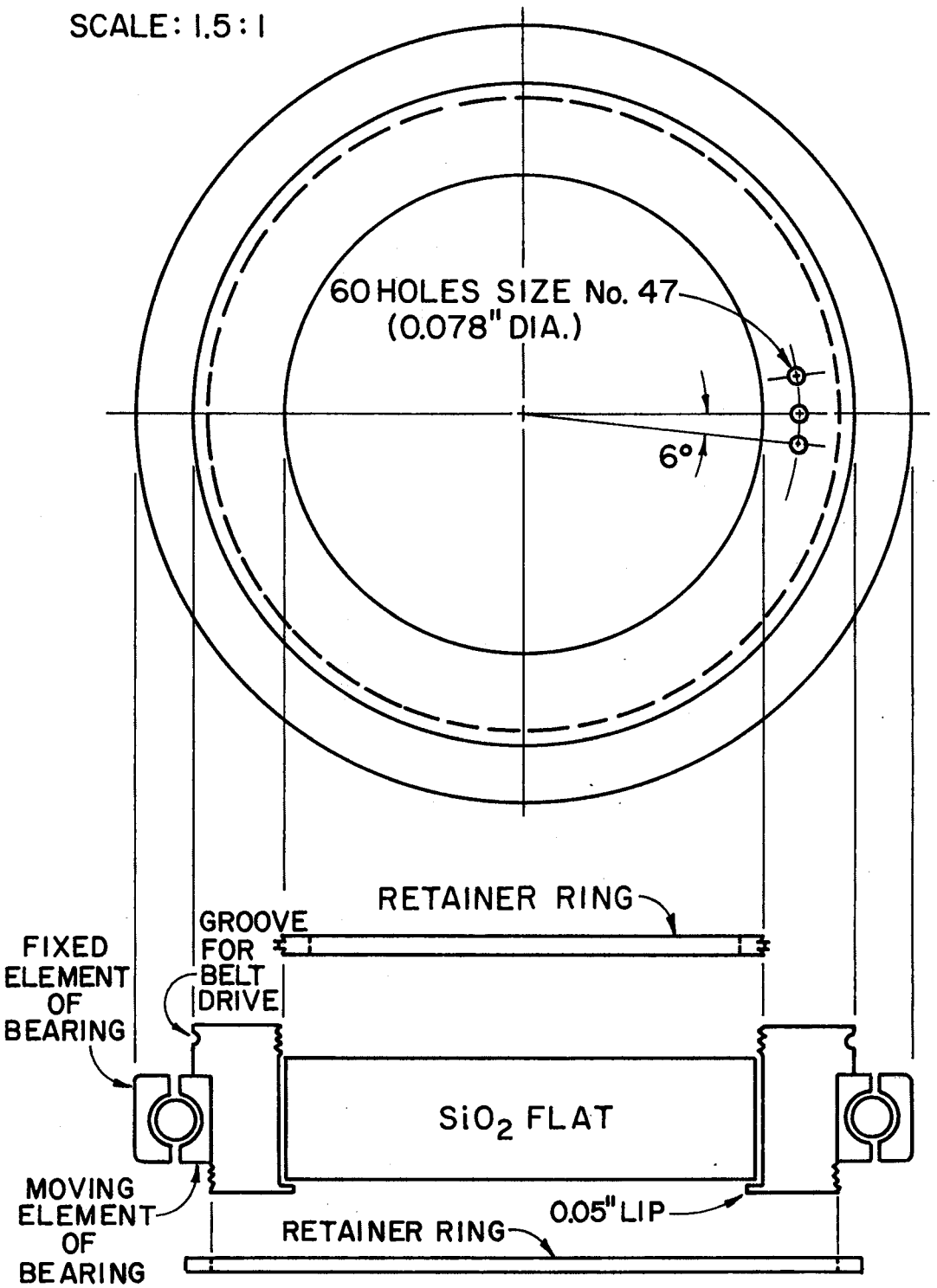

Figure 12. Diagram of Rotator and Optical Flat
(Zavodny, 1970, p. 59)

into a small pile and this is used to lubricate the bearing as it will contain a smaller number of the larger particles than a random sample out of the lubricant container.

The optical flat used for drag measurements was of high quality fused silica manufactured by Amersyl Corporation under the trade name Homosil and supplied by Oriel Optics. This optical flat is designated #1 in Table II and the compensator flat is #2. Optical flat numbers 3 and 4 were used in checking the Brewster angle setting apparatus for repeatability statistics (see Appendix C).

The motor and motor drive system used to rotate the optical flat were the same as used by Zavodny except the constant voltage transformer was manufactured by Raytheon Model RVA125.

To insure consistent positioning of the fused silica disk (if for some reason, such as cleaning, it had to be removed) before the annular retaining ring was secured with the 6 screws the drive belt was made taut and then the bearing was screwed down securely.

Rotation Rate Measuring System

As was the case in Zavodny's work, the rotator sleeve had 60 small evenly spaced holes drilled through it (see Figure 12). An RCA 40598A LED (light-emitting diode) was mounted below and a phototransistor MDR3051 mounted above the sleeve, as shown in Figure 10 and diagrammed in Figure 13. The chopped infrared beam was detected and amplified with the phototransistor to a level greater than 0.1 volt RMS. The signal was then counted by a General Radio Model 1150-BP electronic counter, as mentioned above.

TABLE II

OPTICAL FLAT SPECIFICATIONS

Item Number	Supplier	Surface Flatness	Parallelism (arc sec)	Diameter (inch)	Thickness (inch)
1	Oriel Optics	$\lambda/20$	1	2.000	0.5029
2	Special Optics	$\lambda/10$	5	2.000	0.4866
3	Oriel Optics	$\lambda/20$	1	2.000	0.3902
4	Oriel Optics	$\lambda/20$	1	2.000	0.3923

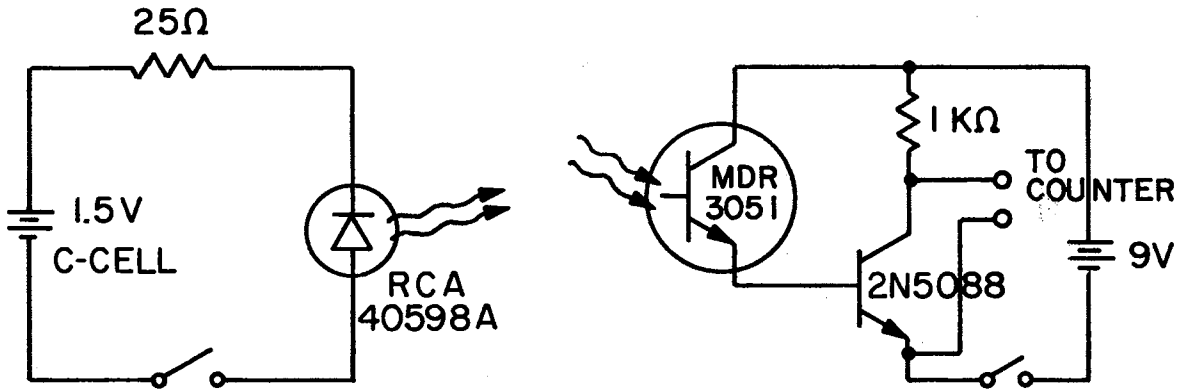

Figure 13. Schematic Diagram of the Rotation Rate Instrumentation System

Equipment Used in Measurement of Optical Length of Ring

The length L of the ring laser cavity was determined by observing the beat frequencies between four axial modes, while the ring was loaded with both the drag disk and the compensator flat. A block diagram and description of equipment setup appears in Zavodny's thesis. The part of the laser beam that was reflected downward from the surface of the compensator flat was directed to the window of an RCA 7107 photomultiplier tube the output of which was displayed on a Tektronix Model 1L20 spectrum analyzer plug-in in a Tektronix Model 585 oscilloscope. The output of a General Radio unit oscillator Type 1208-B powered by a General Radio unit power supply Type 1203-B was both displayed on the 1L20 spectrum analyzer and counted on a Hewlett-Packard Model 524D electronic counter. Two plug-in units were used with the HP 524D counter which were Models 525A and 525C. The equipment mentioned in this chapter are listed in Table III.

TABLE III

PRIMARY EQUIPMENT UTILIZED IN THE EXPERIMENTS

Equipment Name	Manufacturer	Subsystem
Plasma Tube	PEK Labs	Ring Laser
RF Transmitter	Viking	Ring Laser
Mirrors	Laser Optics Inc.	Ring Laser
Granite Block	Texas Granite Corp.	Ring Laser Platform
Photomultiplier	RCA	Beat Frequency Detection
Motor	Electro-Craft	Moving Medium
Motor Control	Electro-Craft	Moving Medium
$\lambda/20$ Optical Flat	Oriel Optics	Moving Medium
$\lambda/10$ Optical Flat	Special Optics	Compensator
$\lambda/20$ Optical Flat (2 each)	Oriel Optics	θ_B Measurement
Oscilloscope	Tektronix	Beat Frequency Detection
Wave Analyzer	Hewlett Packard	Beat Frequency Detection
Spectrum Analyzer	Singer	Beat Frequency Detection
Plug-In	Singer	Beat Frequency Detection
Electronic Counter	General Radio	Beat Frequency Detection
Electronic Counter	General Radio	Beat Frequency Detection
Electronic Counter	Hewlett Packard	Axial Mode Measurement
Frequency Converter Plug-In	Hewlett Packard	Axial Mode Measurement
Unit Oscillator	General Radio	Axial Mode Measurement

CHAPTER IV

EXPERIMENTAL PROCEDURE AND PERIPHERAL MEASUREMENTS

Introduction

This chapter will deal with the evaluation procedure for the parameters required in the calculation of the drag coefficient α (see Equations (2-13) and (2-14)). Also of concern here are other hidden parameters such as setting of the Brewster angle θ_B, location of the center of rotation of the drag disk, repeatability checks as well as details of the preparation of the drag disk. The setting of the normal angle θ_n was discussed in Chapter III because it was intimately associated with preparation of the drag site which was covered there. The following is a discussion of the procedures followed in determining the required parameters.

Thickness and Index of Refraction of Drag Disk

Table V in Chapter V itemizes the desired parameters that enter into the evaluation of the drag coefficient α. The physical dimensions of the fused silica disk were checked and found to be those reported by Zavodny (1970).

The inaccessibility of the necessary equipment to measure the index of refraction n and the dispersion $dn/d\lambda$ of the fused silica disk

with the required accuracy dictated that we rely on the most accurate information available in the literature for these parameters (see Rodney and Spindler, 1954). A four point interpolation of $n(\lambda)$ was computed using values given by Rodney and Spindler for a temperature of $24^{\circ}C$ (this was approximately the room temperature during the experiments). The values used in the interpolation were $\lambda = 0.61$ μm, $\lambda = 0.62$ μm, $\lambda = 0.63$ μm, and $\lambda = 0.64$ μm with $n = 1.457769$, $n = 1.457456$, $n = 1.457156$ and $n = 1.456868$, respectively (see bottom Table V for statement on interpolated values for n). The value of n for $\lambda = 0.633$ μm was computed to be $n = 1.45707$. The dispersion was computed using an equation given by Rodney and Spindler and was found to be $dn/d\lambda = -0.02906\ (\mu m)^{-1}$. The temperature dependence of n was negligible (i.e., $dn/dT = 1 \times 10^{-5}(^{\circ}C)^{-1}$ at $\lambda = 0.6$ μm and $T = 30^{\circ}C$) and the error for the data given by Rodney and Spindler as stated by them do not exceed $\pm 1 \times 10^{-5}$.

Preparation of Drag Disk

It was absolutely necessary that both optical flats be extremely clean because: (a) minimum scattering from the surface of the disk was imperative since scattering tends to increase the lock-in frequency (see Killpatrick, 1967), (b) improperly cleaned disks introduce losses in the ring laser such that oscillation would be prohibited, and (c) a nonuniform surface on the drag disk creates large amplitude fluctuations in the beat frequency signal, such that in bad cases, periodically the signal may be totally blanked out. Dust and visible particles were first removed from the flat by a blast of dry air from a pressurized canister distributed by Century Laboratories under the trade name of Omit. The

surface was then wetted completely with spectrophotometric grade acetone and a sheet of nonabrasive, lint-free lens-cleaning tissue was dragged across the surface removing the acetone and leaving a minimum residue. This was repeated several times and then the solvent was changed to spectrophotometric grade isopropyl alcohol and the process repeated several more times. The compensator flat was treated in another process to insure minimum loss in the ring. In the case of the compensator flat, cleanliness is more important than uniformity of the layer of residue that inevitably remains on the disk's surface because when it is positioned in the laser cavity it need not be removed or repositioned. Therefore, one can control its position such that the entry point of the laser beam produces minimum scatter. To insure maximum cleanliness possible with existing equipment a thin layer of non-plasticized collodion was spread over the surface of the flat and allowed to become rubbery at which time this film of collodion was peeled off. This process was repeated as many as 15 times on each side of the flat. The collodion process seemed to effectively magnify any non-uniformities in the surface of the drag disk perhaps by some of the collodion remaining in small scratches or surface blemishes. Just before the drag disk was mounted several applications of pure ethyl alcohol were made by wetting the surface and dragging the lens cleaning tissue across. This provided a non-visible uniform film on the surface of the disk.

While recording data it was noticed that there was a gradual increase in scattering at the surface of the disk. Dust would occasionally drift and land on the disk which was blown off with a blast of dry air from the above-mentioned canister. The aerosol propellant from the canister seemed to be the source of this apparent buildup of a film and

required one to clean the disk periodically, usually after the recording of data for two curves. This insured consistent data and was adopted as a general procedure in the data taking process.

Setting of the Brewster Angle

To obtain statistics on the repeatability of setting the angle of the platform (hence the angle of the disk) relative to the laser beam at the Brewster angle, one necessarily had to first determine the characteristics of the angular control of the platform (see sine table in Figure 11). Prior to mounting the drag platform on the laser table the angular displacement of the platform was measured using a linear 1 mW laser manufactured by Spectra Physics Model 132. The platform and laser were positioned as shown in Figure 14 and placed on the floor of the laboratory to provide maximum distance from the platform to the ceiling of the room. The mean distance from the reflection point on the disk to the ceiling was 3.05 m. The spot size on the ceiling was 2.5 mm in diameter. The angle of the platform was set roughly to the Brewster angle such that it could be adjusted above and below the desired angle. To obtain an estimate of the precision with which one could set the angle, the micrometer setting was changed by a specific amount and then the distance traveled by the spot on the ceiling was recorded. The micrometer control was adjusted from 0 to 13 mm and the mean change in the distance between spots on the ceiling for a 1 mm change in the micrometer was 2.75 cm. Therefore, a 1 mm change in the micrometer produces a 0.517 degree change in the angle of the platform; in other words, a 0.01 mm change in the micrometer produces less than 20 sec. of arc change in the platform angle.

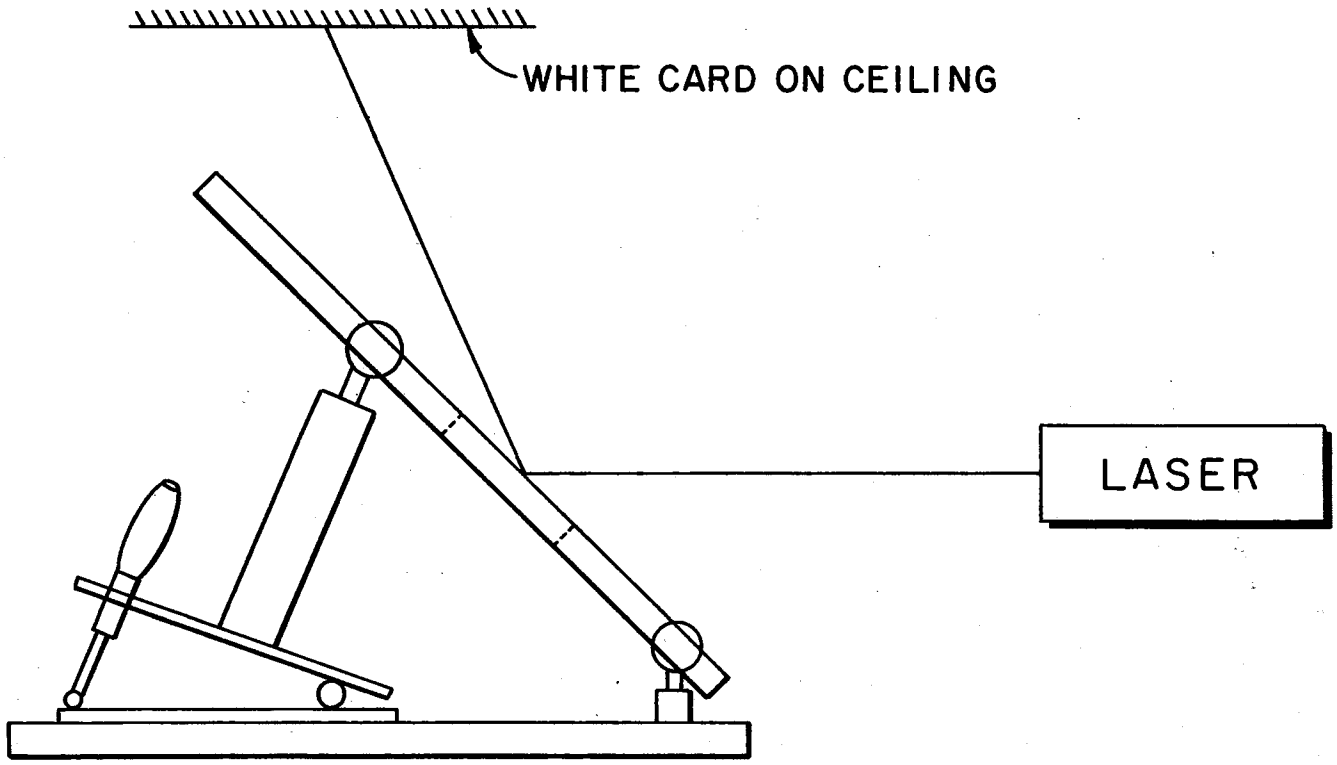

Figure 14. Diagram of Drag Platform Angular Displacement Calibration

After the platform had been mounted on the granite table (setting of θ_n, see Chapter III), the final setting of the angle of the platform, i.e., to set the optical flat to the Brewster angle θ_B the intensity of the reflected beam off the flat was measured with a United Detector PIN-IOD photodiode. The output of the photodiode was fed directly to a Hewlett-Packard HO5-312A wave analyzer. The angle of the platform was then adjusted for a minimum voltage reading on the wave analyzer which is the Brewster angle. Since the wave analyzer does not measure a dc signal, the laser beam had to be intensity modulated. The modulation of the beam was accomplished with a Hewlett-Packard Model 200A audio oscillator. The details of this process follow.

To determine the accuracy with which the Brewster angle of the fused silica optical flat could be adjusted, a polarizing filter supplied by University Laboratories was placed in the path of the reflection, of the elliptically polarized ring laser beam, from the surface of the disk and the intensity measured while adjusting the angle of the platform (see Figure 15). According to Brewster's law (Born and Wolf, 1970), there is an angle at which the electric vector of the reflected light has no component in the plane of incidence and that angle is termed the Brewster angle. However, if there is a component perpendicular to the plane of incidence, the photodiode does not differentiate between the two polarizations. To eliminate such perpendicularly polarized light a polarizing filter was used in the optical circuit after the beam was reflected from the face of the disk. Furthermore, there was considerable light from the spontaneous emission of the plasma tube that was reflected by the laser mirrors and optical flat along with the laser light which tended to decrease the definitiveness of the minimum that

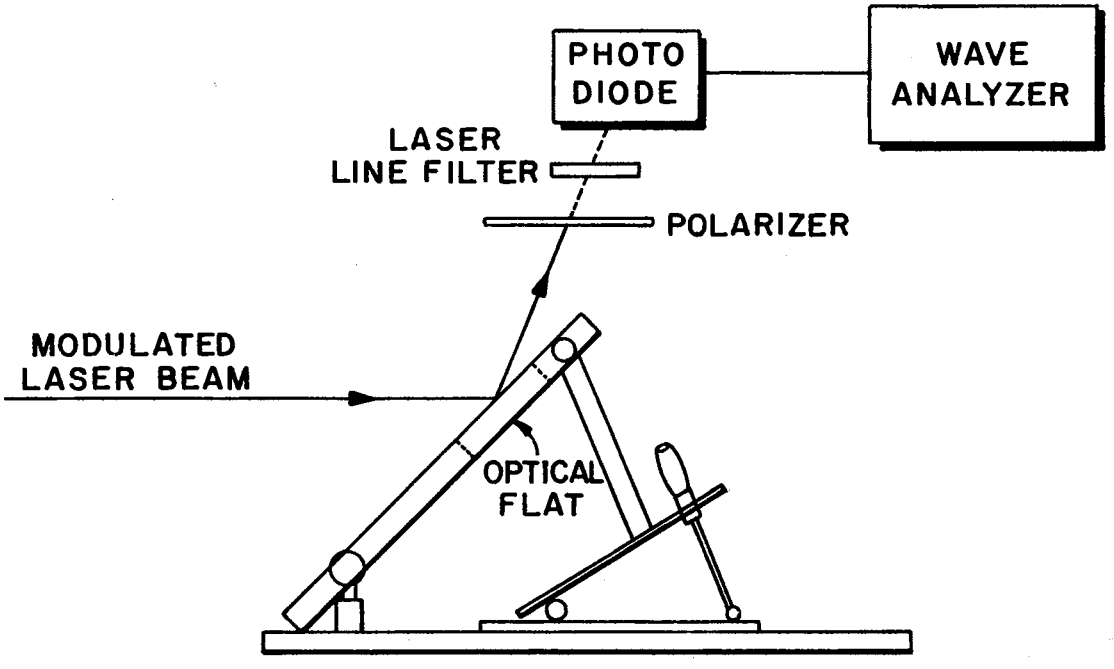

Figure 15. Diagram of θ_B Adjustment Setup

occurs when the disk is at the Brewster angle. To overcome this background light a University Laboratories laser line filter Number 1UL-3021 with a 100 Å bandwidth was mounted in front of the sensitive area of the photodiode. This greatly increased the depth of the minimum when the disk was adjusted through the Brewster angle and increased the accuracy to which this angle could be determined. It must be kept in mind that it was not necessary to know the numerical value of the angle but only to be sure that the disk was at the Brewster angle relative to the laser beam to a specified accuracy. The initial statistics of the repeatability of adjusting to the Brewster angle were obtained using optical flat number 3 and 4 in Table II. The RF transmitter was modulated at approximately 1000 Hz which intensity-modulated the ring laser beam. The photodiode detector was enclosed in an opaque container with a narrow slit mounted over the light sensitive area of the diode. The position of the slit could be adjusted.

One set of 23 data points was taken without the polarizing filter and 4 data runs with between 10 and 19 points were taken with the polarizer in the optical circuit for comparison purposes. All of these data were taken with the 3/8 inch thick disks but after the statistics had been established one data run was made with the Homosil disk that was used for the drag measurements. When the correct micrometer setting for the disk to be at the Brewster angle was established, the angular controls were rigidly fixed and never moved. The data from these measurements is provided in Appendix B. It was found that the Brewster angle could be determined to within an equivalent of 0.02 mm on the micrometer which translates (see above) to 40 seconds of arc. This indicates that the Brewster angle could be determined to within 0.01 degrees.

Measurements of L Through Beat Frequencies of Axial Modes

The procedure for measuring the optical length of the ring laser entails measuring the frequency separation Δf_L of the axial modes. The technique for this measurement was applied by BZ and is discussed in Zavodny's thesis. Once Δf_L is obtained (see Appendix A) the optical length L is given by

$$\Delta f_L = \frac{c}{L} \tag{4-1}$$

The following values were found for the three axial mode beats: $\overline{\Delta f}_{L1}$ = 89.455 MHz, $\overline{\Delta f}_{L2}$ = 2(89.455) MHz, and $\overline{\Delta f}_{L3}$ = 3(89.454) MHz. The mean Δf_L was found to be $\overline{\overline{\Delta f}}_L$ = 89.455 ±0.001 MHz. This yields a value for the optical length L = 3.35133 m ±0.00003 m. The uncertainty in L contributes less than 0.001% error in the determination of α_{exp}.

Location of Center of Rotation of the Disk

The location of the rotation center of the optical flat was determined by observing the scattering of the beam spot from the surface of the rotating disk. When the beam spot is at the center of the rotating disk one can visually observe a symmetric pattern of the scattering centers on the surface of the disk. The position readings were taken by fixing the x-translator and adjusting the y-micrometer off center then bringing it back noting the scattering pattern symmetry and recording the micrometer setting when the pattern displayed maximum symmetry. The same procedure was followed by fixing the y-translator and adjusting the x-micrometer. After each attempt the micrometer was read and the value recorded. It was found that the center coordinates x_c and y_c could

be determined to within 0.0004 inches (0.001 cm). The data are provided in Table VI in Chapter V.

Repeatability of Translator Adjustment

A repeatability check was made by choosing an x_o on the disk and repeatedly adjusting to the chosen x_o and measuring Δf_B and f_m at that location each time. This was repeated 10 times with 10 recordings of Δf_B and f_m made each time. The results are tabulated in Table VII in Chapter V.

y-Variation Sensitivity Check

The treatment of drag in a rotating disk after BZ yields the result that the beat frequency is independent of an excursion of the beam off the x-axis. This calculated result is checked here, in the following manner: the y-translator was moved while fixing the x-translator at a given x_o. At each y-position Δf_B and f_m were recorded (see Table VIII). There were 20 data points taken for each y-position. It was found that the average of all measurements, $\overline{\overline{\Delta f_B}} = 10199.5 \pm 1.5$ Hz and $\sigma_{\overline{\Delta f_B}} = 6.7$ Hz. The total excursion covered in the y-direction was 0.5500 inch and x_o was set at $x_o = 0.5000$ inch. Horizontalness of the x-translation can be assumed due to the fact that there was no apparent systematic difference in α_{exp} as x_o was changed. Indeed the values of α_{exp} seemed to vary randomly about the mean with a change in x_o (see Table XIX in Chapter V).

Procedure for Obtaining Δf_B, f_m and x_o Data

The beat frequency Δf_B was obtained by varying the parameters

(x_o or f_m) in Equation (2-12) in two separate ways. One method was to set the off-axis distance (radius of rotation of the optical flat) to a predetermined value and vary the rotation rate f_m in steps with several readings of Δf_B and f_m taken and averaged for each step (change in f_m). The second method was to set f_m to a predetermined value and vary the off-axis distance x_o, again taking several readings of Δf_B and f_m and averaging for each step (change in x_o).

An actual adjustment sequence for drag measurements would proceed as follows: (a) after either the x_o position on the fused silica disk or the rotation rate had been changed to the desired setting, the beat frequency was observed on the Tektronix 547 oscilloscope and the spectrum analyzer, (b) the wave analyzer was then tuned to peak its response, (c) the wave analyzer was then tuned to either side of the peak to insure that for a small change above or below the voltage peak the count observed on the electronic counter would decrease substantially, (d) the wave analyzer was repeaked and the data recorded, (e) the numerical readouts of both counters were manually recorded in separate columns after each 10-second counting period (the display time after each count was 5 seconds). Between 20 and 40 data recordings were made for each combination of x_o and f_m. For each setting a family of curves was generated and plotted in Figure 16, Figure 17 and Figure 18 in Chapter V. Tables X through XV, Table XVI and Table XVII are the tabulated representations of the data for Figure 16, Figure 17 and Figure 18, respectively.

CHAPTER V

EXPERIMENTAL RESULTS

Introduction

The measurements were taken on only one specific fused silica optical flat. The objective was to determine the drag coefficient with greater precision than had previously been achieved [other media had already been demonstrated (BZ, 1972 and Macek et al., 1964) to produce drag]. Table IV contains a list of identified measurement errors and Table V is a summary of other data on the drag disk with their respective uncertainties (L has been included for convenience even though it is not information on the disk).

Repeatability of Location of Center of Rotation and Translator Positioning

The accuracy with which the off-axis distance x_o can be determined is only as great as the accuracy with which one can determine the center of rotation of the disk; see however Suggestions for Improvement in Chapter VI. The method used to locate the center of rotation of the disk was discussed in Chapter IV. A series of measurements were taken utilizing that method and a typical run is tabulated in Table VI. The standard deviation of the series of micrometer settings was typically between 0.0003 inch and 0.0005 inch, therefore the resulting error in x_o was typically less than 0.07% (see Table IV).

TABLE IV

MEASUREMENT ERRORS

Parameter	Measurement Limitation of an Individual Measurement[1]	Typical Std. Deviation	Typical Data Mean or Best Value	Percent Error ($\frac{\text{Std. Dev.}}{\text{Mean}} \times 100$)
f_m (RPM)	0.1 RPM	0.1 - 0.3 RPM	250 - 3500 RPM	0.006
Δf_B (kHz)	0.1 Hz	5 Hz	1 - 50 kHz	0.02[2]
x_o (in.)	0.0001 in.	0.0004 in.	0.1 - 0.6 in.	0.07[3]
d (in.)	0.0001 in.	0.00005 in.	0.5 in.	0.01
Δf_L (MHz)	1 Hz	1 kHz	89 MHz	0.001
n[4]	10^{-5}	$< 10^{-4}$	1.45707	< 0.007
λ[5] (μm)	10^{-6} μm	--	0.63300 μm	< 0.002
c[6] (cm/sec)	10^5 cm/sec	--	2.9979×10^{10} cm/sec	< 0.003
$\frac{dn}{d\lambda}$ $(\mu m)^{-1}$	10^{-5}	10^{-5}	0.02906	< 0.03

[1]These limitations were the limitation of the equipment in the case of f_m, Δf_B, x_o, d and Δf_L and in the case of n, λ, c and $dn/d\lambda$ the limitation was in information in the literature.

[2]For f_m = 1500 RPM and x_o = 0.6000 inch (Δf_B = 22.7 kHz) ccw rotation.

[3]For x_o = 0.6000 inch.

[4]Rodney and Spindler (1954). Also see Table V.

[5]Comité International des Poids et Mesures (1973).

[6]E. Condon and H. Odishaw, Handbook of Physics (New York, 1958), pp. 7-11.

TABLE V

DATA ON THE DRAG DISK

Quantity	Symbol		Unit	±Absolute Error
Thickness	d	1.2772	cm	1×10^{-4}
Index of Refraction*	n	1.45707		1×10^{-5}
Dispersion	$dn/d\lambda$	0.02906	$(\mu m)^{-1}$	$<1 \times 10^{-5}$
Wave Length	λ	0.63300	μm	$<1 \times 10^{-5}$
Brewster Angle	θ_B	Adjusted	deg	<0.01
Normal Angle	θ_n	Adjusted	deg	<0.1
Rotation Rate	f_m	200-3500	RPM	0.1
Beat Frequency Range	Δf_B	.7-53	kHz	0.005
Displacement	x_o	0.1000-0.5250	in	0.0001
Ring Optical Path Length	L	3.35133	m	3×10^{-5}

*Note that the values given on page 36 for n used in the four point interpolation were computed by Rodney and Spindler (1954) using the relationship

$$n^2 = 2.979864 + \frac{0.008777808}{\lambda^2 - 0.010609} - \frac{84.06224}{96.00000 - \lambda^2} .$$

They make the statement that the computed values for n are better than the observed values.

TABLE VI

REPEATABILITY OF DETERMINING THE CENTER OF THE FUSED SILICA OPTICAL FLAT

Micrometer Readings for x and y Translation	
x Fixed y Varied (inch)	y Fixed x Varied (inch)
0.1607	0.3034
0.1610	0.3045
0.1614	0.3034
0.1613	0.3045
0.1613	0.3044
0.1611	0.3035
0.1604	0.3043
0.1603	0.3037
0.1608	0.3045
0.1615	0.3045
0.1613	0.3040
0.1604	0.3036
$\bar{y} = 0.1610$	$\bar{x} = 0.3040$
$\sigma_y = 0.0004$	$\sigma_x = 0.0005$

The repeatability with which one could set a given value for the x-position with reasonably constant f_m(RPM) and obtain the desired Δf_B (Hz) was checked by repeatedly setting a value of x_o = 0.4000 inches, then recording Δf_B and f_m. This was done a total of ten times recording ten data points each time. The direction from which x_o was approached was alternated with each attempt to eliminate a possible systematic error. The mean value for each set of ten data points was computed and is recorded in Table VII. The mean value of $\overline{\Delta f_B}$ of all 100 data points $\overline{\overline{\Delta f_B}}$ = 5154.4 Hz with a standard deviation of σ = 4.5 Hz and the mean value of $\overline{f_m}$ was $\overline{\overline{f_m}}$ = 501.2 RPM with a standard deviation of σ = 0.1 RPM. This indicates that the beat frequency produced by the setting of x_o was accurate to within 1 x 10^{-3}%.

The degree of sensitivity to a variation on the y-direction was checked before and after the beat frequency data were accumulated. Before any Δf_B or x_o data were recorded, a total excursions in the y-direction with a fixed x-position was made and a maximum deviation in Δf_B of 5 Hz out of 5000 Hz was observed. This was checked again after all beat frequency data was recorded. The sensitivity check results are tabulated in Table VIII (see also Chapter IV).

Determination of Beat Frequency and Rotation Rate

The determination of the drag produced beat frequency Δf_B and the rotation rate of the disk f_m was approached utilizing the two methods discussed in Chapter IV. Each data point plotted in the figures which follow represent the mean of a set of 20 to 40 data accumulated for the specific conditions represented. The raw data for a typical data point

TABLE VII

Δf_B(Hz) REPEATABILITY CHECK FOR SETTING x_o

Run Number	$\overline{\Delta f_B}$(Hz)	σ_i(Hz)	$\overline{f_m}$(RPM)	σ_i(RPM)
1.	5156.0	3.9	501.3	0.09
2.	5153.9	9.6	501.2	0.08
3.	5153.3	5.4	501.1	0.08
4.	5153.5	3.5	501.2	0.10
5.	5152.4	3.6	501.3	0.08
6.	5154.5	4.1	501.4	0.08
7.	5152.9	5.6	501.3	0.09
8.	5153.6	4.7	501.1	0.11
9.	5155.4	4.9	501.4	0.07
All Data (100 Data)	5154.4	4.5	501.2	0.13

x_o = 0.4000 inch

TABLE VIII

SENSITIVITY TO VARIATION IN y-DIRECTION*

x_o (inch)	y_o (inch)	$\overline{\Delta f_B}$ (Hz)	$\sigma_{\overline{\Delta f_B}}$ (Hz)	$\overline{f_m}$ (RPM)	$\sigma_{\overline{f_m}}$ (RPM)
0.5000	+0.3653**	10197.1	7.0	802.2	0.07
0.5000	+0.2153	10200.8	7.4	802.0	0.09
0.5000	+0.1153	10200.7	6.3	801.8	0.10
0.5000	-0.0347	10199.8	5.7	801.8	0.08
0.5000	-0.1847	10199.1	6.9	802.1	0.07
$\overline{\overline{\Delta f_B}}$ (Hz) = 10199.5 Hz				$\overline{\sigma}$ (Hz) = 6.7 Hz	
$\overline{\overline{f_m}}$ (RPM) = 802.0 RPM				$\overline{\sigma}$ (RPM) = 0.08 RPM	

*Total y-excursion = 0.55 inch.

**(+) indicates above y center and (-) indicates below y center.

are represented in Table IX. They are used to obtain the coordinates of one data point (x_o, Δf_B). The 27 data points tabulated there were taken consecutively under the same conditions (so far as was possible) and averaged to give the values represented as one point on one of the plotted curves (in this case Figure 16). Note that a minus sign in f_m represents ccw rotation of the disk. The standard deviation of f_m amounts to less than 0.01% of $\overline{f_m}$ and that of Δf_B is approximately 0.02% of $\overline{\Delta f_B}$, which are typical values. The errors contributed to α_{exp} by data randomness are thus negligible.

Data obtained by maintaining a constant off-axis distance x_o and varying f_m are plotted in Figure 16 and tabulated in Tables X through XV. The data obtained by maintaining a constant f_m while varying x_o are plotted in Figure 17 and Figure 18 and tabulated in Table XVI and Table XVII, respectively. Both cw and ccw rotation of the disk were utilized in lieu of positive and negative positioning of the disk (physical construction of the drag platform prohibited the latter). For the family of curves that resulted from varying f_m, six values of x_o were used from x_o = 0.1000 inch to x_o = 0.5250 inch and Δf_B varied from 0.7 kHz to 20 kHz. For the families of curves that resulted from varying x_o, eleven values of f_m were used from f_m = 500 RPM to f_m = 3500 RPM while the range of Δf_B was from 1.2 kHz to 53 kHz.

An analysis of the data was made using a Hewlett-Packard HP9820 desk calculator. A computer program employing standard least squares linear regression curve fitting was used. The program fit the data to a straight line in the form $y = m_i x + b$ ($i = 0, 1$)(see Equations (2-15) and (2-16)) where x represents the quantity f_m or x_o and y represents the quantity Δf_B. The program printed out the parameters m_i, Δm_i, b, Δb and

TABLE IX

RAW DATA FOR A TYPICAL[1] DATA POINT (x_o, Δf_B)

f_m (RPM)	Δf_B (Hz)
$\overline{f_m}$ = 1500.9	$\overline{\Delta f_B}$ = 22762
$\sigma_{\overline{f_m}}$ = 0.2 RPM	$\sigma_{\overline{\Delta f_B}}$ = 6 Hz
-1500.5	22767
-1500.8	22765
-1500.7	22759
-1500.8	22751
-1501.0	22752
-1501.0	22754
-1501.1	22758
-1501.1	22762
-1501.0	22762
-1501.0	22759
-1501.0	22756
-1501.0	22765
-1501.1	22773
-1501.1	22760
-1501.0	22770
-1501.0	22772
-1501.0	22758
-1501.2	22759
-1500.7	22758
-1500.9	22759
-1500.8	22763
-1500.9	22767
-1501.0	22761
-1500.9	22764
-1500.9	22766
-1500.9	22763
-1501.0	22760

[1]This data was taken with x_o = 0.6000 inch, f_m = 1500 RPM and counterclockwise rotation.

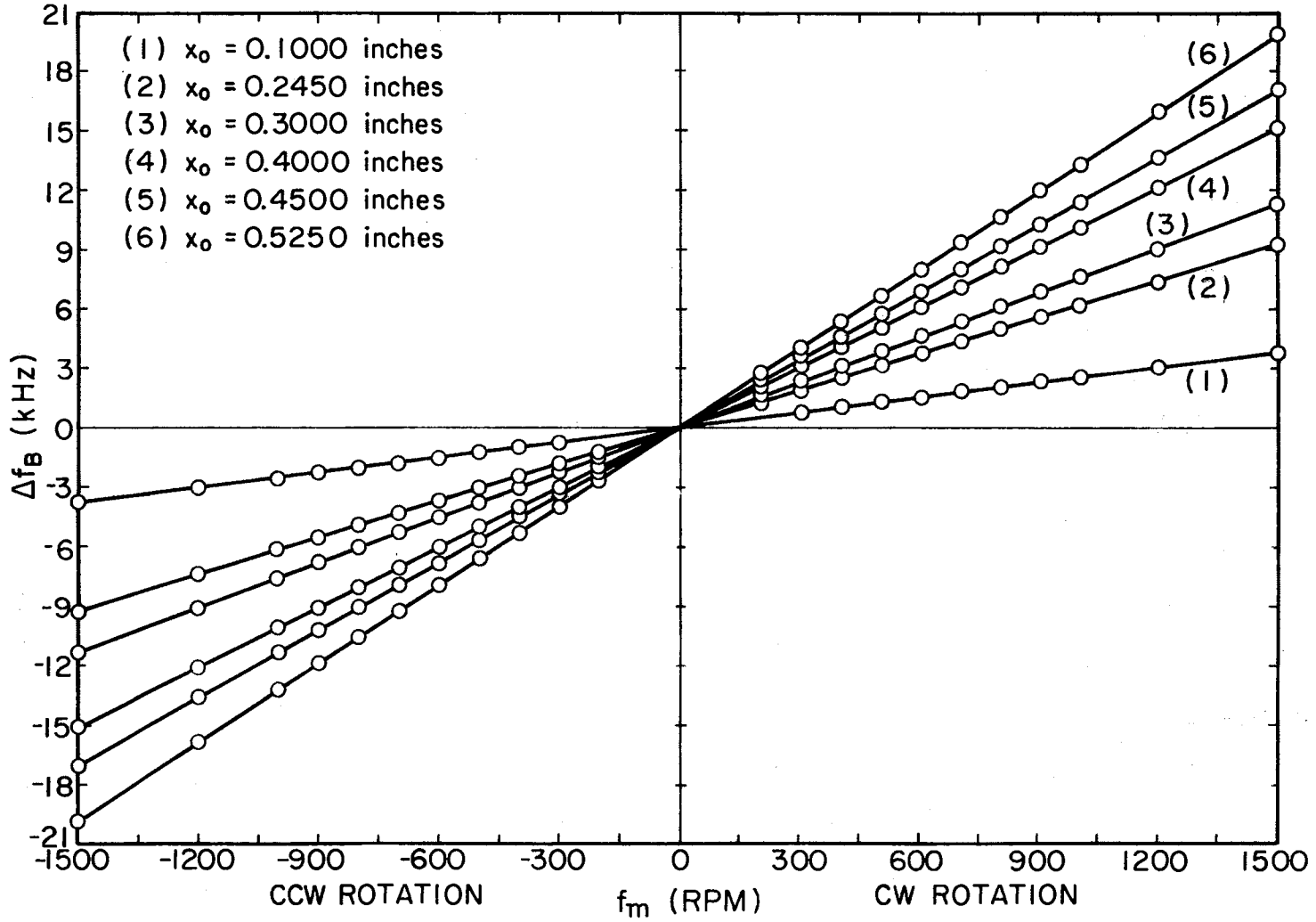

Figure 16. Beat Frequency (Δf_B) vs. Rate of Rotation (f_m)

TABLE X

TABULAR REPRESENTATION OF FIGURE 16

$\overline{f_m}$ Observed (RPM)	$\overline{\Delta f_B}$ Observed (Hz)	Δf_B Fitted (Hz)	DELTA Δf_B (Hz)
1501.2	3852.9	3851.9	1.0
1202.1	3090.3	3093.2	-2.9
1002.6	2584.9	2587.1	-2.2
902.6	2319.7	2333.4	-13.7
802.0	2092.4	2078.2	14.2
702.9	1827.9	1826.8	1.1
602.9	1572.8	1573.2	-0.4
502.6	1321.0	1318.7	2.3
401.6	1060.8	1062.5	-1.7
303.1	812.5	812.6	-0.1
-301.7	-713.8	-721.6	7.8
-401.8	-978.6	-975.5	-3.1
-502.2	-1213.8	-1230.2	16.4
-602.0	-1480.2	-1483.4	3.2
-703.6	-1737.6	-1741.1	3.5
-802.5	-1972.9	-1992.0	19.1
-903.4	-2238.5	-2248.0	9.5
-1000.8	-2581.5	-2495.1	-86.4
-1202.5	-2993.0	-3006.7	13.7
-1501.6	-3746.8	-3765.5	18.7

x_o = .1000"

TABLE XI

TABULAR REPRESENTATION OF FIGURE 16

$\overline{f_m}$ Observed (RPM)	$\overline{\Delta f_B}$ Observed (Hz)	Δf_B Fitted (Hz)	DELTA Δf_B (Hz)
1502.9	9369.7	9371.8	-2.1
1202.2	7508.8	7506.1	2.7
1001.1	6250.2	6258.3	-8.1
902.7	5660.9	5647.8	13.1
801.4	5032.2	5019.3	12.9
702.2	4405.4	4403.8	1.6
602.9	3790.6	3787.6	3.0
502.0	3169.9	3161.6	8.3
402.3	2534.8	2543.0	-8.2
302.7	1920.3	1925.0	-4.7
202.4	1304.1	1302.7	1.4
-202.8	-1214.0	-1211.4	-2.6
-302.3	-1885.1	-1828.8	-56.3
-402.0	-2457.8	-2447.4	-10.4
-502.2	-3058.3	-3069.1	10.8
-603.1	-3687.3	-3695.1	7.8
-702.9	-4319.8	-4314.4	-5.4
-802.0	-4900.0	-4929.2	29.2
-903.0	-5556.4	-5555.9	-0.5
-1001.7	-6161.9	-6168.3	6.4
-1201.9	-7413.9	-7410.5	-3.4
-1501.7	-9266.0	-9270.6	4.6

x_o = .2450"

TABLE XII

TABULAR REPRESENTATION OF FIGURE 16

$\overline{f_m}$ Observed (RPM)	$\overline{\Delta f_B}$ Observed (Hz)	Δf_B Fitted (Hz)	DELTA Δf_B (Hz)
1501.7	11455.7	11449.2	6.5
1201.6	9172.0	9170.6	1.4
1001.3	7655.9	7649.8	6.1
902.5	6897.1	6899.6	-2.5
802.0	6144.6	6136.5	8.1
703.0	5382.5	5384.8	-2.3
603.2	4618.6	4627.1	-8.5
501.9	3861.1	3857.9	3.2
402.5	3104.1	3103.2	0.9
302.6	2347.0	2344.7	2.3
201.9	1562.1	1580.1	-18.0
-202.3	-1512.3	-1488.9	-23.4
-302.5	-2246.6	-2249.7	3.1
-402.0	-3001.4	-3005.2	3.8
-502.0	-3757.7	-3764.5	6.8
-601.8	-4525.6	-4522.3	-3.3
-701.5	-5281.2	-5279.3	-1.9
-802.6	-6033.8	-6046.9	13.1
-901.5	-6797.4	-6797.8	0.4
-1001.1	-7547.0	-7554.1	7.1
-1201.3	-9082.6	-9074.2	-8.4
-1502.4	-11354.9	-11360.4	5.5

x_o = .3000"

TABLE XIII

TABULAR REPRESENTATION OF FIGURE 16

$\overline{f_m}$ Observed (RPM)	$\overline{\Delta f_B}$ Observed (Hz)	Δf_B Fitted (Hz)	DELTA Δf_B (Hz)
1501.9	15252.2	15253.1	-0.9
1201.8	12214.0	12215.2	-1.2
1001.8	10185.4	10190.6	-5.2
901.2	9183.5	9172.2	11.3
802.1	8158.5	8169.0	-10.5
701.3	7165.3	7148.6	16.7
601.7	6146.1	6140.4	5.7
502.4	5129.2	5135.1	-5.9
402.2	4119.8	4120.8	-1.0
301.0	3103.0	3096.4	6.6
201.9	2084.0	2093.2	-9.2
-202.4	-1999.1	-1999.5	0.4
-301.9	-3014.6	-3006.8	-7.8
-402.0	-4023.7	-4020.1	-3.6
-502.0	-5039.8	-5032.4	-7.4
-601.2	-6045.3	-6036.6	-8.7
-701.5	-7046.0	-7051.9	5.9
-802.3	-8076.1	-8072.3	-3.8
-901.6	-9062.5	-9077.5	15.0
-1001.0	-10081.2	-10083.8	2.6
-1202.2	-12120.1	-12120.5	0.4
-1501.5	-15149.8	-15150.3	0.5

x_o = .4000"

TABLE XIV

TABULAR REPRESENTATION OF FIGURE 16

$\overline{f_m}$ Observed (RPM)	$\overline{\Delta f_B}$ Observed (Hz)	Δf_B Fitted (Hz)	DELTA Δf_B (Hz)
1501.8	17158.9	17154.3	4.6
1201.8	13740.8	13736.6	4.2
1003.1	11465.7	11472.9	-7.2
902.2	10313.9	10323.4	-9.5
801.4	9184.3	9175.1	9.2
702.1	8037.0	8043.8	-6.8
603.0	6918.7	6914.9	3.8
502.2	5765.0	5766.5	-1.5
401.0	4612.9	4613.6	-0.7
301.2	3488.2	3476.7	11.5
201.8	2345.2	2344.3	0.9
-202.1	-2270.1	-2257.1	-13.0
-301.7	-3387.6	-3391.8	4.2
-401.5	-4535.0	-4528.7	-6.3
-501.8	-5674.4	-5671.4	-3.0
-602.1	-6817.4	-6814.0	-3.4
-702.0	-7954.4	-7952.1	-2.3
-803.3	-9098.7	-9106.2	7.5
-902.3	-10234.6	-10234.0	-0.6
-1001.7	-11355.7	-11366.4	10.7
-1201.2	-13638.7	-13639.2	0.5
-1503.4	-17084.7	-17081.9	-2.8

x_o = .4500"

TABLE XV

TABULAR REPRESENTATION OF FIGURE 16

$\overline{f_m}$ Observed (RPM)	$\overline{\Delta f_B}$ Observed (Hz)	Δf_B Fitted (Hz)	DELTA Δf_B (Hz)
1502.8	20020.9	20011.8	9.1
1202.4	16016.4	16021.6	-5.2
1001.9	13354.5	13358.4	-3.9
902.5	12040.2	12038.0	2.2
802.1	10700.3	10704.4	-4.1
702.2	9384.7	9377.2	7.5
601.7	8046.1	8042.5	3.6
501.0	6699.7	6704.9	-5.2
400.7	5374.4	5372.6	1.8
302.8	4055.6	4072.2	-16.6
202.1	2734.6	2734.6	0.0
-202.4	-2633.7	-2638.4	4.7
-302.2	-3971.6	-3964.1	-7.5
-401.9	-5282.7	-5288.4	5.7
-500.7	-6596.8	-6600.8	4.0
-602.0	-7945.7	-7946.4	0.7
-701.9	-9262.7	-9273.3	10.6
-802.3	-10600.4	-10607.0	6.6
-902.0	-11939.7	-11931.3	-8.4
-1001.4	-13258.0	-13251.6	-6.4
-1201.9	-15912.0	-15914.9	2.9
-1503.1	-19917.8	-19915.7	-2.1

x_o = .5250"

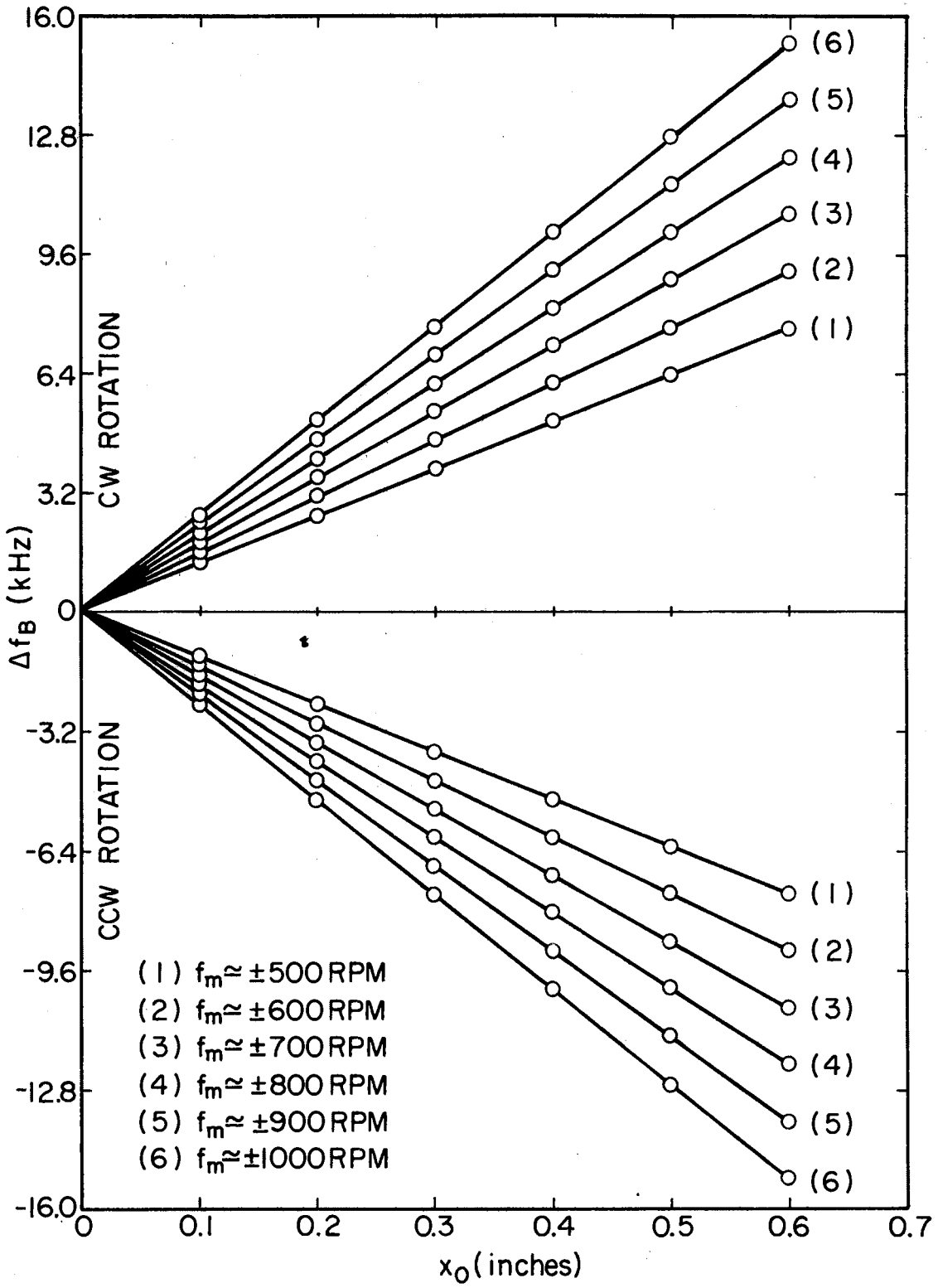

Figure 17. Beat Frequency (Δf_B) vs. Off-Axis Distance (x_o)

TABLE XVI

TABULAR REPRESENTATION OF FIGURE 17

x_o Observed (inch)	$\overline{f_m}$ (RPM)	$\overline{\Delta f_B}$ Observed (Hz)	Δf_B Fitted (Hz)	DELTA Δf_B (Hz)
.6000	500.5	7634.0	7645.2	-11.2
.5000	500.5	6376.6	6378.6	-2.0
.4000	500.4	5126.4	5112.0	14.4
.3000	500.8	3848.2	3845.4	2.8
.2000	501.0	2585.6	2578.8	6.8
.1000	500.9	1308.0	1312.2	-4.2
.1000	-500.4	-1225.3	-1221.0	-4.3
.2000	-500.9	-2495.5	-2487.6	-7.9
.3000	-501.1	-3759.8	-3754.2	-5.6
.4000	-500.4	-5005.7	-5020.8	15.1
.5000	-500.7	-6287.6	-6287.4	- .2
.6000	-500.6	-7558.0	-7554.0	-4.0
.6000	600.5	9170.8	9169.4	1.4
.5000	600.8	7654.4	7648.7	5.7
.4000	600.4	6126.1	6128.0	-1.9
.3000	601.2	4607.4	4607.3	.1
.2000	601.2	3082.5	3086.7	-4.2
.1000	600.6	1564.2	1566.0	-1.8
.1000	-600.8	-1471.9	-1475.4	3.5
.2000	-601.3	-3006.1	-2996.0	-10.1
.3000	-601.2	-4514.2	-4516.7	2.5
.4000	-600.7	-6034.3	-6037.4	3.1
.5000	-600.8	-7564.3	-7558.1	-6.2
.6000	-600.4	-9070.8	-9078.7	7.9
.6000	701.7	10716.3	10713.2	3.1
.5000	701.6	8930.8	8936.0	-5.2
.4000	701.7	7166.8	7158.7	8.1
.3000	701.8	5376.5	5381.4	-4.9
.2000	701.9	3610.0	3604.2	5.8
.1000	702.3	1825.2	1826.9	-1.7
.1000	-702.6	-1729.9	-1727.6	-2.3
.2000	-701.8	-3515.6	-3504.8	-10.8
.3000	-702.2	-5287.3	-5282.1	-5.2
.4000	-702.0	-7052.6	-7059.4	6.8
.5000	-701.6	-8831.0	-8836.6	5.6
.6000	-702.0	-10613.1	-10613.9	0.8

TABLE XVI (Continued)

x_o Observed (inch)	$\overline{f_m}$ (RPM)	$\overline{\Delta f_B}$ Observed (Hz)	Δf_B Fitted (Hz)	DELTA Δf_B (Hz)
.6000	802.6	12227.9	12220.5	7.4
.5000	801.9	10203.4	10191.9	11.5
.4000	801.9	8154.7	8163.3	-8.6
.3000	801.3	6124.4	6134.8	-10.4
.2000	801.8	4106.8	4106.2	0.6
.1000	800.9	2068.3	2077.6	-9.3
.1000	-801.4	-1984.3	-1979.5	-4.8
.2000	-801.2	-4003.6	-4008.1	4.5
.3000	-801.9	-6036.2	-6036.6	0.4
.4000	-801.1	-8055.0	-8065.2	10.2
.5000	-802.4	-10084.9	-10093.8	8.9
.6000	-802.4	-12132.7	-12122.3	-10.4
.6000	903.1	13770.3	13768.0	2.3
.5000	902.8	11479.7	11481.9	-2.2
.4000	903.7	9187.3	9195.8	-8.5
.3000	903.1	6909.0	6909.8	- .8
.2000	902.6	4630.6	4623.7	6.9
.1000	903.8	2342.0	2337.6	4.4
.1000	-903.3	-2244.4	-2234.5	-9.9
.2000	-903.1	-4506.6	-4520.6	14.0
.3000	-903.0	-6807.1	-6806.7	- .4
.4000	-902.9	-9097.9	-9092.8	-5.1
.5000	-902.7	-11370.6	-11378.9	8.3
.6000	-903.4	-13673.9	-13665.0	-8.9
.6000	1003.0	15285.7	15295.6	-9.9
.5000	1002.7	12751.8	12754.5	-2.7
.4000	1003.0	10224.0	10213.5	10.5
.3000	1003.0	7683.6	7672.4	11.2
.2000	1002.8	5133.1	5131.4	1.7
.1000	1002.9	2584.4	2590.3	-5.9
.1000	-1003.0	-2496.3	-2491.8	-4.5
.2000	-1002.6	-5030.5	-5032.8	2.3
.3000	-1003.2	-7576.9	-7573.9	-3.0
.4000	-1003.6	-10119.2	-10114.9	-4.3
.5000	-1003.3	-12654.4	-12656.0	1.6
.6000	-1003.0	-15194.0	-15197.0	3.0

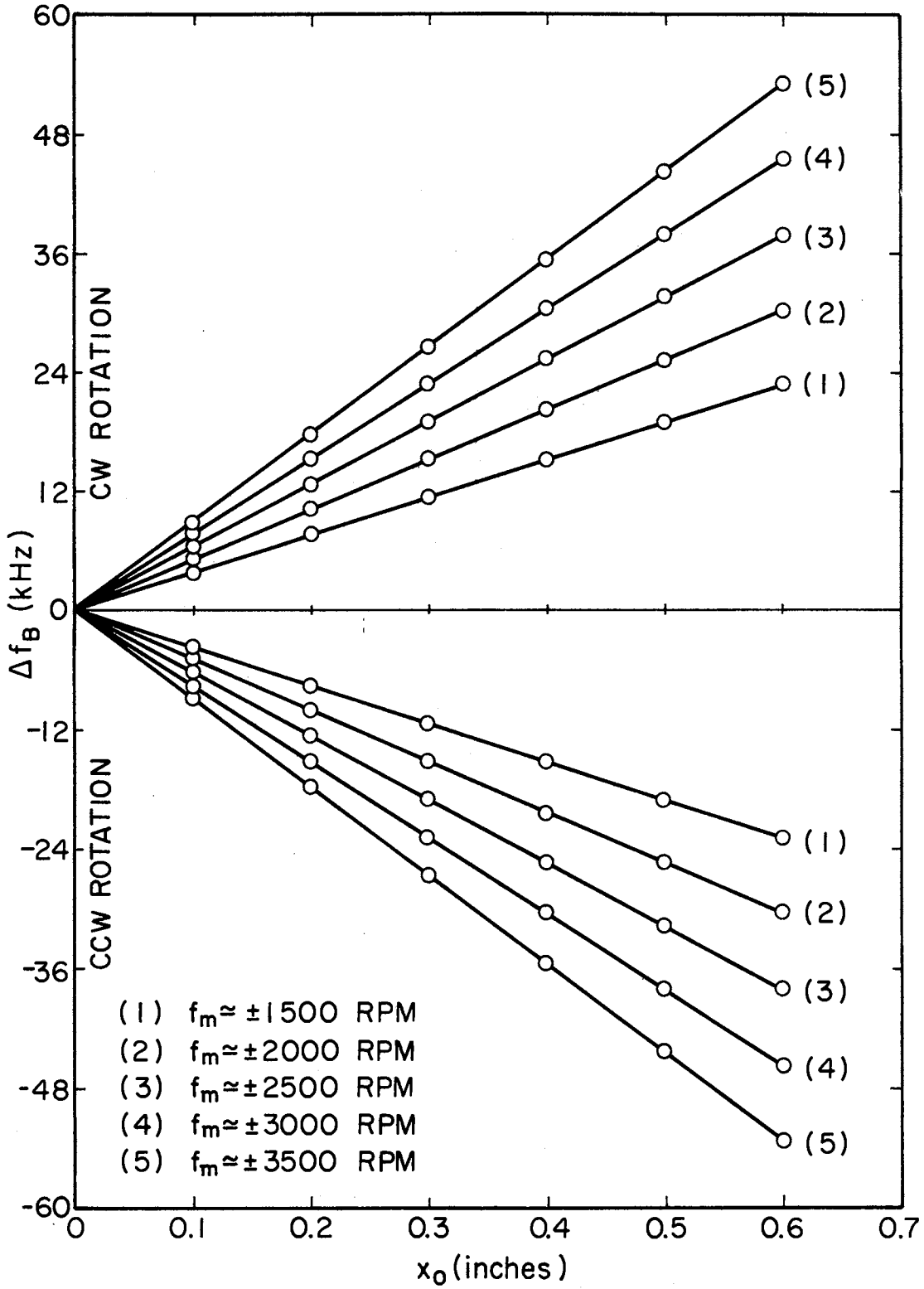

Figure 18. Beat Frequency (Δf_B) vs. Off-Axis Distance (x_o)

TABLE XVII

TABULAR REPRESENTATION OF FIGURE 18

x_o Observed (inch)	$\overline{f_m}$ (RPM)	$\overline{\Delta f_B}$ Observed (Hz)	Δf_B Fitted (Hz)	DELTA Δf_B (Hz)
.6000	1500.8	22863.9	22863.2	.7
.5000	1500.6	19058.6	19061.0	-2.4
.4000	1500.7	15250.2	15258.8	-8.6
.3000	1501.3	11470.2	11456.6	13.6
.2000	1501.2	7651.1	7654.3	-3.2
.1000	1500.3	3855.1	3852.1	3.0
.1000	-1500.4	-3755.0	-3752.3	-2.7
.2000	-1500.5	-7553.8	-7554.5	.7
.3000	-1500.8	-11354.8	-11356.7	1.9
.4000	-1500.6	-15163.3	-15159.0	-4.3
.5000	-1500.3	-18961.3	-18961.2	- .1
.6000	-1500.9	-22762.0	-22763.4	1.4
.6000	2001.0	30427.5	30434.1	-6.6
.5000	2000.8	25369.5	25369.6	- .1
.4000	2000.3	20297.8	20305.0	-7.2
.3000	2000.7	15243.1	15240.5	2.6
.2000	2000.8	10185.9	10176.0	9.9
.1000	2000.5	5114.8	5111.4	3.4
.1000	-2000.5	-5012.4	-5017.7	5.3
.2000	-2001.0	-10082.1	-10082.2	.1
.3000	-2000.2	-15146.9	-15146.8	- .1
.4000	-2001.1	-20213.2	-20211.3	-1.9
.5000	-2000.2	-25272.9	-25275.9	3.0
.6000	-2001.1	-30348.8	-30340.4	-8.4
.6000	2500.4	38023.9	38024.3	- .4
.5000	2500.8	31689.4	31695.7	-6.3
.4000	2501.1	25371.0	25367.0	4.0
.3000	2500.4	19027.8	19038.4	-10.6
.2000	2500.7	12708.7	12709.7	-1.0
.1000	2501.5	6397.0	6381.1	15.9
.1000	-2501.0	-6279.1	-6276.2	-2.9
.2000	-2501.4	-12599.9	-12604.9	5.0
.3000	-2500.0	-18921.3	-18933.5	12.2
.4000	-2501.1	-25269.5	-25262.2	-7.3
.5000	-2501.3	-31591.7	-31590.8	- .9
.6000	-2501.8	-37927.1	-37919.5	-7.6

TABLE XVII (Continued)

x_o Observed (inch)	$\overline{f_m}$ (RPM)	$\overline{\Delta f_B}$ Observed (Hz)	Δf_B Fitted (Hz)	DELTA Δf_B (Hz)
.6000	3002.5	45686.7	45681.3	5.4
.5000	3002.4	38067.8	38075.9	-8.1
.4000	3002.5	30467.1	30470.6	-3.5
.3000	3001.5	22874.0	22865.2	8.8
.2000	3002.6	15263.6	15259.8	3.8
.1000	3002.6	7654.7	7654.5	.2
.1000	-3002.4	-7561.8	-7556.2	-5.6
.2000	-3002.5	-15157.5	-15161.6	4.1
.3000	-3002.2	-22780.7	-22767.0	-13.7
.4000	-3002.9	-30370.9	-30372.3	1.4
.5000	-3002.7	-37980.0	-37977.7	-2.3
.6000	-3002.4	-45573.6	-45583.0	9.4
.6000	3502.6	53165.2	53163.3	1.9
.5000	3502.6	44315.6	44310.7	4.9
.4000	3502.1	35456.5	35458.0	-1.5
.3000	3501.7	26607.7	26605.4	2.3
.2000	3501.9	17765.7	17752.8	12.9
.1000	3502.8	8884.8	8900.1	-15.3
.1000	-3502.1	-8813.1	-8805.2	-7.9
.2000	-3502.0	-17674.0	-17657.8	-16.2
.3000	-3501.8	-26509.7	-26510.4	.7
.4000	-3502.8	-35355.2	-35363.1	7.9
.5000	-3502.3	-44207.1	-44215.7	8.6
.6000	-3502.6	-53066.5	-53068.3	1.8

correlation information from which one could compute r. The terms m_i and b are the slope and y-axis intercept, respectively, of the fitted straight line. The terms Δm_i and Δb are the deviations of the estimated values of m_i and b, respectively, from the data. The term r is the correlation coefficient between the data and the least squares fitted line, i.e., r is defined as

$$r = \frac{1}{N} \sum \left(\frac{x - \bar{x}}{\sigma_x}\right) \left(\frac{y - \bar{y}}{\sigma_y}\right). \tag{5-1}$$

Determination of α_{exp} and Comparison with Theoretical Models

The slopes m_o and m_1 have different units. So that one can compare these two sets of slopes, we introduce new quantities M_i, such that

$$M_o = \frac{m_o}{x_o} \tag{5-2}$$

and

$$M_1 = \frac{m_1}{f_m} \quad . \tag{5-3}$$

The numerical values of the M_o's and the M_1's should be equal, within their statistical error. The drag coefficient α_{exp} is then obtained, through Equations (2-13b) and (2-14b), directly from the M_i's as

$$\alpha = \left(\frac{\lambda L}{4\pi d n}\right) M_i = K M_i \, , \; i = 0, 1 \tag{5-4}$$

where M_i is here assumed to have the units m^{-1}. Note that K absorbs all quantities which are kept constant in the experiments. Since α_{exp} is expected to be independent of rotation rate and off-axis distance on the disk, the distribution of all M_i's gave direct evidence of the quality of the measurements, specifically, the distributions of M_o and M_1 should

overlap if no significant systematic errors in x_c (location of rotation center) and f_m occurred. For the relative errors of M_i we obtain, after differentiation of the definitions in Equations (5-2) and (5-3),

$$\frac{\Delta M_i}{M_i} = \frac{\Delta m_i}{m_i} . \tag{5-5}$$

the maximum deviation for M_i from the mean value for all data is 0.052 $Hz(RPM)^{-1}inch^{-1}$. The average error in M_i of all data is ΔM_i = 0.009 $Hz(RPM)^{-1}inch^{-1}$ or 0.036% of M_i. Hence, since α_{exp} is directly proportional to M_i (and therefore m_i), the errors inherent in α_{exp} due to randomness in M_i should be less than 0.04%.

The values of the correlation coefficient r, all except one, being greater than 0.9999 indicate that deviation from a straight line is negligible.

The drag coefficient α_{exp} was calculated from the M_i [note that $M_i \left(\frac{Hz}{RPM\ inch}\right)\left(\frac{6000}{2.54}\right) = M_i(m^{-1})$] values in Table XVIII using Equation (5-4), whereby the quantities λ, L, d, n are taken from Table V. The The results in terms of α_{exp} are listed in Table XIX, where they are compared with both the Lorentz and Laub drag coefficients. The calculated numerical values for α_{Lo} and α_{La} were obtained by using Equation (2-5) and Equation (2-7), respectively, with n, λ and $dn/d\lambda$ from Table V and were found to be α_{Lo} = 0.5416 and α_{La} = 0.5376. The Fresnal drag coefficient α_F was calculated utilizing Equation (2-5) minus the dispersion term and was found to be α_F = 0.5290.

The value of α_{Lo} deviates from the value of $\bar{\alpha}_{exp}$ by 0.2% and the value of α_{La} deviates from the value $\bar{\alpha}_{exp}$ by 0.9%. Figure 19 is a histogram of all experimentally obtained drag coefficients, with a Gaussian distribution superimposed. The cell width is 0.0002 and N is the number of

TABLE XVIII

COMPUTED TERMS FOR A LEAST SQUARES FIT TO A STRAIGHT LINE $y = m_i x + b$

Data Identification	m_i	Δm_i	M_i $\left(\frac{\text{Hz}}{\text{RPM inch}}\right)$	ΔM_i $\left(\frac{\text{Hz}}{\text{RPM inch}}\right)$	b (Hz)	Δb (Hz)	r
(Δf_B vs. x_o)	(Hz/inch) (i=1)	(Hz/inch) (i=1)	(i=1)	(i=1)			
$\overline{f_m}$ = 500.7 RPM	12666	6	25.297	0.013	45.6	2.5	0.999999
$\overline{f_m}$ = 600.8 RPM	15207	4	25.311	0.006	45.3	1.6	0.999999
$\overline{f_m}$ = 701.9 RPM	17773	5	25.321	0.006	49.7	1.8	0.999999
$\overline{f_m}$ = 801.7 RPM	20286	7	25.303	0.008	49.1	2.6	0.999999
$\overline{f_m}$ = 903.1 RPM	22861	6	25.314	0.006	51.5	2.3	0.999999
$\overline{f_m}$ = 1003.0 RPM	25410	5	25.334	0.005	49.3	1.9	0.999999
$\overline{f_m}$ = 1500.7 RPM	38022	4	25.336	0.003	49.9	1.6	0.999999
$\overline{f_m}$ = 2000.7 RPM	50645	4	25.314	0.002	46.9	1.6	0.999999
$\overline{f_m}$ = 2501.0 RPM	63286	6	25.304	0.002	52.4	2.4	0.999999
$\overline{f_m}$ = 3002.4 RPM	76054	5	25.331	0.002	49.1	2.1	0.999999
$\overline{f_m}$ = 3502.3 RPM	88526	7	25.277	0.002	47.5	2.7	0.999999
(Δf_B vs. f_m)	(Hz/RPM) (i=0)	(Hz/RPM) (i=0)	(i=0)	(i=0)			
x_o = 0.1000 inch	2.5368	0.006	25.368	0.060	43.7	5.1	0.99991
x_o = 0.2450 inch	6.2046	0.004	25.325	0.020	46.9	3.4	0.99996
x_o = 0.3000 inch	7.5928	0.002	25.309	0.006	47.1	1.9	0.99978
x_o = 0.4000 inch	10.1230	0.002	25.308	0.005	49.4	1.7	0.99998
x_o = 0.4500 inch	11.3923	0.002	25.316	0.004	45.3	1.4	0.99992
x_o = 0.5250 inch	13.2831	0.002	25.301	0.004	50.0	1.4	0.99998

$\overline{M_i}$ = 25.316 Hz/(RPM inch) $\qquad$ $\overline{b}$ = 48.2 Hz

$\overline{\Delta M_i}$ = 0.009 Hz/(RPM inch) $\qquad$ $\overline{\Delta b}$ = 2.2 Hz

TABLE XIX

COMPARISON OF EXPERIMENTAL AND THEORETICAL DRAG COEFFICIENTS

Figure Number	x_o (inch)	$\overline{f_m}$ (RPM)	α_{exp} (measured)	Percent Deviation From Theoretical Value $\left(\frac{\alpha_{exp} - \alpha^*_{La}}{\alpha_{La}}\right) \times 100(\%)$	Percent Deviation From Theoretical Value $\left(\frac{\alpha_{exp} - \alpha^{**}_{Lo}}{\alpha_{Lo}}\right) \times 100(\%)$
17		500.7	0.5421	0.84	0.09
17		600.8	0.5424	0.89	0.15
17		701.9	0.5426	0.93	0.18
17		801.7	0.5422	0.86	0.11
17		903.1	0.5425	0.91	0.17
17		1003.0	0.5429	0.99	0.24
18		1500.7	0.5430	1.00	0.26
18		2000.7	0.5425	0.91	0.17
18		2501.0	0.5423	0.87	0.13
18		3002.4	0.5428	0.97	0.22
18		3502.3	0.5417	0.76	0.02
16	0.1000		0.5436	1.12	0.37
16	0.2450		0.5427	0.95	0.20
16	0.3000		0.5424	0.89	0.15
16	0.4000		0.5423	0.87	0.13
16	0.4500		0.5425	0.91	0.17
16	0.5250		0.5422	0.86	0.11
All Data Averages		$\overline{\alpha}_{exp} = 0.5425$ ($\sigma_{\overline{\alpha}_{exp}} = 0.0004$)		0.91	0.17

*$\alpha_{Lo} = 0.5416$ **$\alpha_{La} = 0.5376$

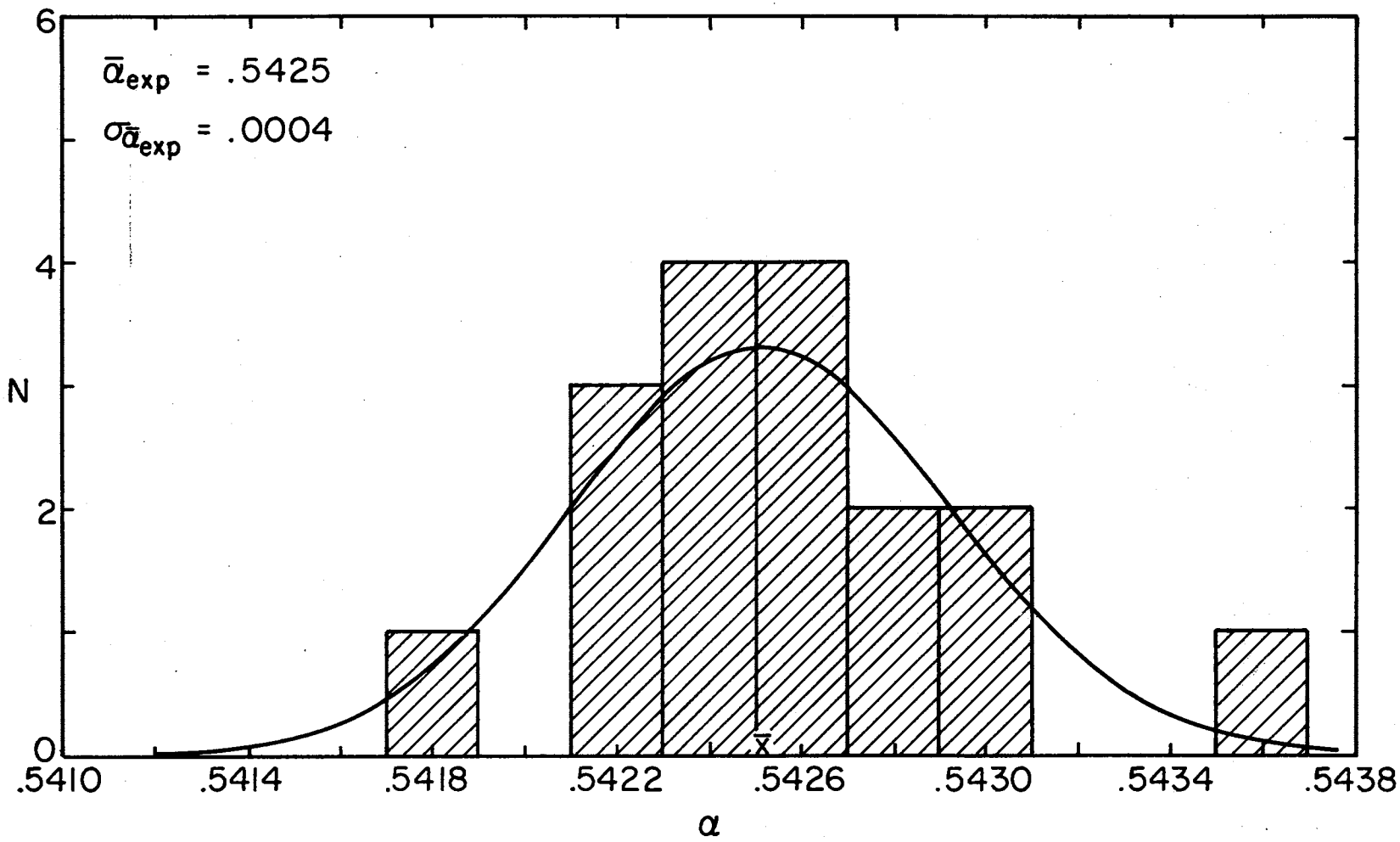

Figure 19. Histogram of the Seventeen Experimentally Obtained Drag Coefficient α_{exp}

α_{exp}'s in each cell. Note that the greatest deviation from the average value obtained for α_{exp} occurred at the extremes of both x_o and f_m. The smallest value was $\alpha_{exp} = 0.5417$ which resulted from $f_m = 3502.3$ RPM. At this (the highest) RPM the inherent modulation of the beat frequency signal, probably due to vibration, increased in depth to a condition where some counts could have been lost when the percent of modulation approached 100%. This would cause the slope of the curve to be smaller that it should have been which would cause α_{exp} to be smaller also. An explanation of the largest value of α_{exp}, at $x_o = 0.1000$ inch, is more difficult. It could have occurred due to an uncertainty in the center of rotation of the disk, but was probably due to one "data point" at $f_m = -1000.8$ RPM (see Table X). A curve was fitted without this point included and the slope changed such that the value of α_{exp} moved left of the center of the distribution. This point was included, however, because all Δf_B, x_o and f_m data were recorded and included in the averages presented, which prevents any arbitrary selection of experimental data.

CHAPTER VI

CONCLUSIONS AND SUGGESTIONS FOR IMPROVEMENT

Conclusions

The primary objective of this endeavor was to determine the Fresnel drag coefficient in a ring laser to a greater degree of accuracy than had previously been accomplished. This was to be accomplished by reducing certain of the error sources in the work done by Zavodny (1970). Statistical averaging of the data was used to reduce (where possible) the effect of the errors. The major reduction of error sources was accomplished by redesigning the x-y positioning equipment and developing new techniques for setting the Brewster angle θ_B. All other errors were kept equal to or less than the levels established in the Zavodny experiments. Under optimum conditions, the total errors involved in the measurements reported herein were less than 0.2%.

Seventeen curves were plotted using the experimental data. The slopes of these curves were then used to determine the drag coefficient from either Equation (2-13b) or Equation (2-14b). The seventeen α_{exp}'s had an average of $\overline{\alpha}_{exp} = 0.5425$ with a standard deviation of $\sigma_{\overline{\alpha}_{exp}} = 0.0004$. Considering the theoretical aspect, PD pointed out that the conditions of these experiments should lead to the Lorentz formula. The comparison is, therefore, very interesting: $\overline{\alpha}_{exp}$ discriminates against both of the two viable theoretical models, namely, α_{Lo} and α_{La} and clearly discriminates against the Fresnel (without dispersion) drag

coefficient α_F. The Lorentz model α_{Lo} is only a few σ's away from $\overline{\alpha}_{exp}$ but the Laub model α_{La} is as much as 12 σ's away from $\overline{\alpha}_{exp}$. The difference expressed as a percentage of the dispersion terms was 7.8% for α_{Lo} and 57.3% for α_{La}. In the light of these experimental results it appears that none of the existing theoretical models account for the actual drag in the ring laser. Note that there is a difference in the α_{Lo} in this work and the value considered in both the BZ and PD papers. This is due to two changes: First, the value for dispersion used in those papers had to be slightly changed (see reference in Table IV), second, the most recent value for λ introduces a smaller change in the value for α_{Lo}.

Suggestions for Improvement

The vibrational instabilities encountered in these experiments tended to scatter the beat frequency data more than the state-of-the-art would suggest should occur. Killpatrick (1967) was able to measure the Sagnac effect with an accuracy of ±0.1 Hz; of course, this was done without introducing a moving medium in the ring cavity. It is suggested that this accuracy could be achieved if the ring laser were kept extremely vibration free. This would require complete enclosure of the ring, isolating it from the moving air. Ideally the enclosure would be evacuated to some pressure less than atmospheric pressure. Also, the table on which the drag platform rests must be completely isolated mechanically and acoustically from the ring laser. An air bearing of some kind for the rotator would solve much of the vibration difficulties. Imperfections in the surface of the optical flat (even though it was extremely high quality it had been cleaned many times and irregularities

inevitably appeared) can be overcome to a large extent by operating the ring laser in the infrared mode, at either 1.15 μm or 3.39 μm at these wavelengths the system is less sensitive to dust particles and imperfections in the moving medium. Experiments were performed by this author with the ring laser oscillating at $\lambda = 1.15$ μm using a Judson indium arsenide photovoltiac detector to detect the beat frequency with quite impressive results (not reported herein) so far as the insensitivity to dust and surface blemishes on the disk are concerned. The primary objective in reducing data scattering is that this would allow one to reduce or eliminate signal filtering and processing which is essential if an improvement in accuracy is to be obtained. These wavelengths and the techniques discussed herein would make possible drag measurements on liquids with much greater precision than has been achieved before. Every effort should be made to completely eliminate the wave analyzer in the data processing path.

The accuracy of the x-y translator was not exhausted in these experiments but could be if one develops a more accurate technique of determining the center of rotation of the optical flat. It is suggested that the need to locate the center can be eliminated by positioning the disk in a number of random locations (not just on the $y = 0$ axis) and recording Δf_B and f_m, then processing the data such that the x-position is found relative to any other x-position and not relative to the center of rotation. Utilizing this technique one could obtain maximum accuracy from the x-y translator.

The detection of the fringe shifting after the two beams coupled out of the laser cavity have been superimposed can be greatly enhanced. This can be accomplished by designing a lens utilizing the back surface

of the output mirror of the ring laser such that the output beams form plane waves. This would provide well defined straight line fringes when the two beams are superimposed, rather than the curved fringes normally seen. The minimum achievement here would be a greatly improved interference pattern.

BIBLIOGRAPHY

Aharoni, Joseph. The Special Theory of Relativity. Oxford: Clarendon Press, 1959.

Anderson, James L. Principles of Relativity Physics. New York: Academic Press, 1967.

Bagaev, S. N., Y. V. Troitskii, and B. I. Troshin. "The Polarization of Radiation and the Frequency Characteristics of Ring Lasers With a Triangular Resonator." Opt. Spectr. USSR., 21 (1966), 420-421.

Barnes, Frank S. Laser Theory. New York: IEEE Press, 1972.

Bergmann, Peter G. Introduction to the Theory of Relativity. New York: Prentice-Hall, Inc., 1942.

Bilger, H. R., and A. T. Zavodny. "Fresnel Drag in a Ring Laser: Measurement of the Dispersive Term." Phys. Rev. A, 5 (1972), 591-599.

Born, Max, and Emil Wolf. Principles of Optics. New York: Pergamon Press, 1970.

Comité International des Poids et Mesures. "New Standards for Light Velocity and Wavelength." Physics Today, 27 (1974), 112.

Drude, Paul K. L. The Theory of Optics. New York: Dover, 1959.

Fenster, P., and W. K. Kahn. "An Optical Technique for Measurement of Gas Flow Profiles Utilizing a Ring Laser." Applied Optics, 7 (1968), 2383-2391.

Fizeau, H. L. Comptes Rendus, 33 (1851), 349; "Sur les Hypothèses Relatives a l'Etère Lumineaux." Ann. Chem. Phys., 57 (1859), 385-404.

Fox, A. G., and T. Li. "Modes in a Maser Interferometer With Curved and Tilted Mirrors." Proc. IEEE, 51 (1963), 80-89.

Fresnel, A. "Sur l'Influence du Mouvement Terrestre dans Quelques Phénomènes d'Optique." Ann. Chem. Phys., 9 (1818), 57.

Haress, F. "Die Geschwindigkeit des lichtes in bewegten Körpern." (Unpub. dissertation, Jena, 1912.)

Heer, C. V. "Resonant Frequencies of an Electromagnetic Cavity in an Accelerated System of Reference." Phys. Rev., 134 (1964), A799-A804.

Hutchings, T. J., J. Winocur, R. H. Durrett, E. D. Jacobs, and W. L. Zingery. "Amplitude and Frequency Characteristics of a Ring Laser." Phys. Rev., 152 (1966), 467-473.

Javan, A., E. A. Ballik, and W. L. Bond. "Frequency Characteristics of a CW He-Ne Optical Maser." J. Opt. Soc. Am., 52 (1962), 96-98.

Jenkins, Francis A., and Harvey E. White. Fundamentals of Optics, 3rd ed. New York: McGraw-Hill, 1957.

Killpatrick, J. "The Laser Gyro." IEEE Spectrum, (October, 1967), 44-55.

Klein, Miles V. Optics. New York: John Wiley and Sons, 1970.

Laub, J. "Zur Optik der bewegten Körper." Ann. Physics Leipzig, 25 (1908), 175.

Laue, M. "Die Mitführung des Lichtes durch bewegte Körper nach dem Relativitätsprinzip." Ann. d. Phys., 23 (1907), 989-990.

Lorentz, H. A. Versuch einer Theorie der elektrischen und optischer Erscheinungen in bewegten Körpern. Leiden: Brill, 1895; Lectures on Theoretical Physics, Vol. 3. New York: MacMillan, 1931.

Macek, W. M., and D. T. M. Davis, Jr. "Rotation Rate Sensing With Traveling-Wave Ring Lasers." App. Phys. Letters, 2 (1963), 67-68.

Macek, W. M., J. R. Schneider, and R. M. Salmon. "Measurement of Fresnel Drag With the Ring Laser." J. Appl. Phys., 35 (1964), 2556-2557.

Macek, W. M., and E. J. McCartney. Sperry Engr. Rev., 19 (1966), 8.

Maiman, T. H. "Optical Maser Action in Ruby." Brit. Commun. Electron., 7 (1960), 674-675; "Simulated Optical Radiation in Ruby." Nature, 187 (1960), 493-494.

Marcuse, Dietrich. Light Transmission Optics. New York: Van Nostrand Reinhold Co., 1972.

McFarlane, R. A. "Frequency Pushing and Frequency Pulling in a He-Ne Gas Optical Maser." Phys. Rev., 135 (1964), A543-A550.

Michelson, A. A., and F. W. Morley. Am. J. Sci., 31 (1886), 377.

Parks, W. F., and J. T. Dowell. "Fresnel Drag in Uniformly Moving Media." Phys. Rev. A, 9 (1974), 565-567.

Podgorski, T. J., and F. Aronowitz. "Langmuir Flow Effects in the Laser Gyro." IEEE J. Quant. Electr., GE-4 (1968), 11-18.

Post, E. J. "Sagnac Effect." Rev. Mod. Phys., 39 (1967), 475-493.

Privalov, V. E., and S. A. Fridrikhov. "The Ring Gas Laser." Soviet Physics Uspekhi, 97 (1969), 153-167.

Rigden, J. D., and A. D. White. "The Interaction of Visible and Infrared Maser Transitions in the Helium-Neon System." Proc. IEEE (Corres.), 51 (1963), 943-945.

Rigrod, W. W. "The Optical Ring Resonator." Bell Sys. Tech. J., (1965), 907-916.

Rodney, W. S., and R. J. Spindler. "Index of Refraction of Fused-Quartz Glass for Ultraviolet, Visible, and Infrared Wavelengths." Journal of Research of the National Bureau of Standards, 53 (1954), 185-189.

Rosenthal, A. H. "Regenerative Circulatory Multiple-Beam Interferometry for the Study of Light-Propagation Effects." J. Opt. Soc. Am., 52 (1962), 1143-1148.

Rosser, W. G. V. An Introduction to the Theory of Relativity. London: Butterworth and Co., Ltd., 1964.

Siegman, A. E. An Introduction to Lasers and Masers. New York: McGraw-Hill, 1971.

Sommerfeld, A. Lectures on Theoretical Physics, Optics, Vol. IV. New York: Academic Press, 1954.

Yariv, Amnon. Quantum Electronics. New York: John Wiley and Sons, 1967.

Yariv, Amnon. Introduction to Optical Electronics. New York: Holt, Rinehart and Winston, 1971.

Zavodny, A. T. "A Determination of the Effect of the Dispersive Term on the Fresnel Drag Coefficient Using a Ring Laser." (Unpub. Ph.D. thesis, Oklahoma State University, 1970.)

Zeeman, P. "Fresnel's Coefficient for Light of Different Colours - First Part." Proc. Roy. Acad. Amsterdam, 17 (1914), 445-451; "Fresnel's Coefficient for Light of Different Colours - Second Part." Proc. Roy. Acad. Amsterdam, 18 (1915), 388-408; "On a Possible Influence of the Fresnel-Coefficient on Solar Phenomena." Proc. Roy. Acad. Amsterdam, 18 (1916), 711-715; "An Optical Method for Determining the Ratio Between the Mean and Maximal Velocities in the Turbulent Motion of Fluids in a Cylindrical Tube. Contribution to the Experiment of Fizeau." Proc. Roy. Acad. Amsterdam, 18 (1916), 1240-1247; "Direct Optical Measurement of the Velocity

at the Axis in the Apparatus for Fizeau's Experiment." Proc. Roy. Acad. Amsterdam, 19 (1917), 125-132; "The Propagation of Light in Moving Transparent Solid Substances. I. Apparatus for the Observation of the Fizeau-Effect in Solid Substances." Proc. Roy. Acad. Amsterdam, 22 (1920), 462-465.

Zeeman, P., and A. Smethlage. "The Propagation of Light in Moving Transparent Solid Substances. II. Measurements on the Fizeau-Effect in Quartz." Proc. Roy. Acad. Amsterdam, 22 (1920), 512-522.

APPENDIX A

AXIAL MODE SEPARATION MEASUREMENTS FOR THE RING LASER CONTAINING THE OPTICAL FLAT AND COMPENSATOR FLAT

The following is a sample of the raw data taken in the measurement of the ring optical length L as explained in Chapter IV. It must be kept in mind that L enters linearly in α, therefore, it is more than adequate to measure L to 10^{-5}. The counts were read from the frequency counter and rounded off to that presented here. There were between 72 and 85 readings taken for each Δf_{Li} but only every fifth reading is given in Table XX. The statistical reduced values for Δf_{Li} are summarized in Table II.

TABLE XX

AXIAL MODE SEPARATION BEAT FREQUENCIES Δf_{Li}*

First Beat Frequency Δf_{L1}(kHz)	Frequency Δf_{L2}(kHz)	Frequency Δf_{L3}(kHz)
89,455	178,909	268,362
89,456	178,910	268,361
89,454	178,910	268,361
89,456	178,909	268,361
89,455	178,910	268,360
89,455	178,911	268,360
89,456	178,911	268,360
89,456	178,909	268,360
89,455	178,910	268,360
89,456	178,911	268,361
89,455	178,910	268,360
89,455	178,910	268,361
89,455	178,909	268,361
89,456	178,910	268,362
89,455	178,911	268,360
	178,909	268,360
	178,910	268,361
	178,911	268,361
	178,910	268,360
	178,909	268,360
i = 1	i = 2	i = 3
$\overline{\frac{\Delta f_{Li}}{i}}$ = 89,455 kHz	89,455 kHz	89,454 kHz

*The best estimate of the ring optical path length of L (see Chapter IV) is

$$L = \frac{c}{\frac{1}{3}\sum_{i=1}^{3}\overline{\frac{\Delta f_{Li}}{i}}} = (3.35133 \pm 0.00003)\ \text{m}.$$

APPENDIX B

REPEATABILITY OF SETTING OF THE BREWSTER ANGLE

Several sets of data were taken, for statistical purposes, to determine how closely one could set the angle of the fused silica disk to the Brewster angle. A Hewlett-Packard 312A wave analyzer was used to take voltage readings as a direct indication of the intensity of the beam that was reflected from the surface of the optical flat. The laser plasma tube (beam amplifier) was modulated at 1 kHz to intensity modulate the light beam. This allowed one to use the highly sensitive ac voltmeter (HP-312A) to measure the intensity of the modulated light beam as it was typically less than 10 μ volts. The tabulated data in Table XXI were taken under the same conditions so far as was possible. The accuracy that was obtained was sufficient to set the Brewster angle to within 0.01 degrees. It was found that a 0.01 mm change in the sine table adjustment micrometer (see Figure 11, Figure 14, and Figure 15) produced a 19 second of arc change in the platform angle. Data were taken with both a 1/2 inch thick disk (optical flat #1 in Table II) mounted in the platform and a 3/8 inch thick disk (#3 in Table II) mounted in the platform. The 1/2 inch thick disk was used in the drag measurements.

TABLE XXI

STATISTICAL DATA FOR ESTABLISHING ACCURACY OF θ_B SETTING

Micrometer Settings in mm				
3/8 in. Disk Run Number 1	3/8 in. Disk Run Number 2	3/8 in. Disk Run Number 3	3/8 in. Disk Run Number 4	1/2 in. Disk Run Number 5
10.90	10.85	10.85	10.84	10.62
10.85	10.81	10.89	10.88	10.60
10.85	10.84	10.84	10.87	10.64
10.84	10.89	10.84	10.83	10.65
10.88	10.86	10.83	10.83	10.63
10.86	10.87	10.85	10.86	10.63
10.88	10.86	10.88	10.85	10.64
	10.85	10.85	10.83	10.60
	10.81		10.88	
	10.84		10.85	
	10.84		10.84	
	10.86		10.88	
	10.86		10.87	
	10.85		10.87	
			10.87	
			10.86	
			10.85	
			10.85	
			10.83	
$\text{Mean}_1 = 10.87$ mm*			$\text{Mean}_3 = 10.85$ mm	
$\sigma_1 = 0.02$ mm**			$\sigma_3 = 0.02$ mm	
$\text{Mean}_2 = 10.85$ mm			$\text{Mean}_4 = 10.85$ mm	
$\sigma_2 = 0.02$ mm			$\sigma_4 = 0.02$ mm	
$\text{Mean}_5 = 10.63$ mm				
$\sigma_5 = 0.02$ mm				

*Mean_i = Mean value for run number i.

**σ_i = Standard deviation for run number i.

APPENDIX C

EQUIPMENT USED IN THE EXPERIMENTS

A complete listing of all of the equipment which was used in the experiments reported in this work is given in Table XXII. The code is designated in the footnote following the table.

TABLE XXII

A COMPLETE LIST OF THE EQUIPMENT UTILIZED IN THE EXPERIMENTS

Equipment Name	Manufacturer	Model	Code*
Plasma Tube	PEK Labs	--	1
RF Transmitter	Viking	Challenger	1
Iris Diaphragm	Edmund Scientific	40997	1
Granite Block	Texas Granite Corp.	--	2
Isolation Feet	Korfund	LKA-33 (4 units)	2
Isolation Feet	Korfund	LKA-34 (4 units)	2
Beam Splitter	Edmund Scientific	3197	3
Mirror	Edmund Scientific	30286	3
Bearing	Split Ball Bearing Co.	3 TKR 41-52-U 0-5 Tight	6
Motor	Electro-Craft	E-350M	6
Motor Control	Electro-Craft	E-350MG	6
$\lambda/20$ Optic Flat - Fused Silica	Oriel Optics	A-43-464-80	6
$\lambda/10$ Optic Flat - Fused Silica	Special Optics	10-403-2 III P	7
Lubricant - WSe_2	Cerac	1433	6
Wave Analyzer	Hewlett-Packard	310	4
Plug-In	Singer	UR-3	4
Spectrum Analyzer	Singer	MF-5	4

TABLE XXII (Continued)

Equipment Name	Manufacturer	Model	Code*
Electronic Counter	Hewlett-Packard	524D	8
10-100 MHz Mixer	Hewlett-Packard	525A	8
Signal Generator	Tektronix	190B	11
100-510 MHz Mixer	Hewlett-Packard	525C	8
Spectrum Analyzer	Tektronix	1L20	8
Power Meter	Optics Technology	610	8
He-Ne Laser (1 mw)	Spectra Physics	132	2
Electronic Air Cleaner	Honeywell	F38A	9
x-y Graduated Mechanical Stage	Lansing	20.127	6
Constant Voltage Transformer	Raytheon	RVA 125	5
$\lambda/20$ Optical Flat	Oriel Optics	A-43-564-80 (2 units)	10
Power Supply	Kepco Labs	815B (2 units)	8
Sine Table	Ealing	22-8189	10
Interference Filter	University Labs	ULI 3021 100 Å bw at 6328 Å	10
Oscilloscope	Tektronix	585	4
Oscilloscope	Tektronix	547	8
Plug-In	Tektronix	1A7A	4
Wave Analyzer	Hewlett-Packard	312A	10
Photo Diode	United Detector	PIN-10D	10
Photo Diode	Fairchild	FPM-200	4
Light-Emitting Diode	RCA	RCA 40598A	5
Phototransistor	Motorola	MDR 3051	5
Electronic Counter	General Radio	1150-BP	5
Electronic Counter	General Radio	1151-A	4
Unit Oscillator	General Radio	1208-B	8

*The following is a designation of the code used: Code Number--Subsystem Equipment Was Used In: 1 - Ring Laser; 2 - Ring Laser Platform; 3 - Optical Mixer; 4 - Δf_B (Beat Frequency) Detection; 5 - f_m (Frequency of Rotation) Detection; 6 - Moving Medium; 7 - Compensator; 8 - Δf_{axial} Detection; 9 - Air Filtration; 10 - θ_B Measurement; 11 - Counter Comparison Check.

VITA 2

Walter Kent Stowell

Candidate for the Degree of

Doctor of Philosophy

Thesis: A PRECISION MEASUREMENT OF FRESNEL DRAG IN A RING LASER

Major Field: Electrical Engineering

Biographical:

Personal Data: Born in Reno, Nevada, March 8, 1940.

Education: Graduated from Miami High School, Miami, Oklahoma, May, 1959; received the Bachelor of Science degree from Oklahoma State University with a major in Electical Engineering, January, 1970; received the Master of Science degree from Oklahoma State University with a major in Electrical Engineering, May, 1972; completed requirements for the Doctor of Philosophy degree, July, 1974.

Professional Experience: Graduate Research and Teaching Assistant, Oklahoma State University from January, 1970, through July, 1974.